Journal of Computational Physics 228 (2009) 3025–3047

Contents lists available at ScienceDirect

Journal of Computational Physics

journal homepage: www.elsevier.com/locate/jcp

Third-order Energy Stable WENO scheme

Nail K. Yamaleev [a,*], Mark H. Carpenter [b,1]

[a] Department of Mathematics, North Carolina A&T State University, Greensboro, NC 27411, USA
[b] Computational Aerosciences Branch, NASA Langley Research Center, Hampton, VA 23681, USA

ARTICLE INFO

Article history:
Received 6 March 2008
Received in revised form 2 January 2009
Accepted 8 January 2009
Available online 22 January 2009

Keywords:
High-order finite difference methods
Weighted essentially non-oscillatory schemes
Energy estimate
Numerical stability
Artificial dissipation

ABSTRACT

A new third-order Energy Stable Weighted Essentially Non-Oscillatory (ESWENO) finite difference scheme for scalar and vector hyperbolic equations with piecewise continuous initial conditions is developed. The new scheme is proven to be linearly stable in the energy norm for both continuous and discontinuous solutions. In contrast to the existing high-resolution shock-capturing schemes, no assumption that the reconstruction should be total variation bounded (TVB) is explicitly required to prove stability of the new scheme. We also present new weight functions which drastically improve the accuracy of the third-order ESWENO scheme. Based on a truncation error analysis, we show that the ESWENO scheme is design-order accurate for smooth solutions with any number of vanishing derivatives, if its tuning parameters satisfy certain constraints. Numerical results show that the new ESWENO scheme is stable and significantly outperforms the conventional third-order WENO scheme of Jiang and Shu in terms of accuracy, while providing essentially non-oscillatory solutions near strong discontinuities.

1. Introduction

High-order finite difference weighted essentially non-oscillatory (WENO) schemes have now become a state-of-the-art methodology for solving problems with strong discontinuities that arise in computational fluid dynamics, computational aeroacoustics, computational electromagnetics, and other areas. The WENO schemes have evolved from the successful ENO reconstruction idea which was originally proposed in [1]. In contrast to the ENO reconstruction which adaptively chooses one "smoothest" stencil from p candidate stencils, the WENO schemes use a weighted combination of all the candidate stencils to form the WENO reconstruction of the flux. Each weight is a nonlinear function of so-called smoothness indicators that measure the smoothness of the numerical solution on that particular stencil which this weight has been assigned. If the solution is smooth in all candidate stencils, then the WENO scheme asymptotes to a target scheme which provides either higher order accuracy [2,3] or improved resolution for short waves [4,5]. If the solution is discontinuous in one of the candidate stencils, the WENO scheme effectively nullifies the corresponding weight, thus biasing the stencil away from the discontinuity and successfully emulating the ENO stencil choosing procedure. To date, various WENO schemes have been developed for finite difference [3–7], finite volume [2,8–10], and finite element [11,12] formulations.

Although the high-order WENO schemes have been successfully used for solving a broad spectrum of applied problems, very few theoretical stability proofs for these schemes are available in the literature. It is shown in [3] that the WENO scheme of Jiang and Shu is stable for the conservation law equation $\mathbf{u}_t + \nabla \cdot \mathbf{f}(\mathbf{u}) = 0$, if a smooth flux splitting and a nth-order Runge–Kutta scheme ($n \geqslant 3$) are used, and the differential problem is at least $p + [(d+1)/2] + 2$ times continuously

* Corresponding author. Tel.: +1 336 285 2093; fax: +1 336 256 0876.
E-mail address: nkyamale@ncat.edu (N.K. Yamaleev).

[1] Work partially performed while the second author was in residence at Technical University of Delft, Delft, The Netherlands. Technical monitor Professor Hester Bijl.

0021-9991/$ - see front matter © 2009 Elsevier Inc. All rights reserved.
doi:10.1016/j.jcp.2009.01.011

differentiable (d is the dimensionality of the problem, and p is the order of approximation). For the scalar conservation law equation in one dimension, Jiang and Yu [13] have shown the existence and stability of discrete stationary shocks for the conventional third-order WENO scheme [3], based on the global Lax–Friedrichs flux splitting. Note, however, that for the third-order WENO scheme, the key condition for existence and stability (see Theorem 4.4 in [13]) has been verified numerically only for sample values of the parameter q_0, rather than proven rigorously for all $q_0 \in [0,1]$. Recently, Ferretti [14] as well as Qiu and Shu [15] proved the convergence of a quite general class of self-similar total variation bounded (TVB) schemes to the entropy solution of strictly convex scalar one-dimensional Hamilton–Jacobi and conservation law equations under the large time step assumption: $\Delta t/\Delta x \to +\infty$. This assumption eliminates the need for the cell [16] or wavewise [17] entropy inequality that is traditionally required to prove the convergence of this class of TVB schemes. Note that this time step constraint violates the CFL condition, a natural condition for time-dependent hyperbolic problems (e.g. fluids, acoustics, electromagnetics). Thus, these TVB schemes are only amenable for implicit temporal integrators.

In contrast to nonlinear ENO and WENO formulations, stability proofs for linear schemes are elementary. Indeed, Kriess and Scherer [20] recognized that discrete operators satisfying a summation-by-parts (SBP) condition, are automatically stable in an L_2-energy norm. Furthermore, they noted that the SBP property could be used to *develop* new schemes, not just prove the stability of existing ones. Numerous schemes currently exist that satisfy the SBP property. In addition to weak form FEM operators, SBP operators exist for central schemes [21], Padé schemes [22], upwind schemes [23], and spectral collocation schemes [24–26]. Although proofs of stability exist for linear schemes, robustness is frequently lacking. Because the linear schemes use a fixed stencil, they are susceptible to Gibbs oscillations for discontinuous data.

Another class of L_2-stable methods is discontinuous Galerkin (DG) methods. The DG methods satisfy a cell entropy inequality for the square entropy [18], which implies L_2 stability for a scalar nonlinear conservation law equation. Furthermore, this stability property generalizes to symmetric nonlinear hyperbolic systems [19]. Although the L_2 stability enhances the scheme's linear and nonlinear robustness, it alone does not guarantee solution monotonicity. The high-order DG methods admit spurious oscillations in problems with strong discontinuities, and require additional artificial dissipation in the form of limiters to suppress the oscillations [11,12]. Much still remains unresolved in the development of stability theory for nonlinear equations. What is clear, however, is that construction of suitable artificial dissipation operators is essential when dealing with nonlinear equations, and any mathematical theory that provides guidance for this algorithmic development is beneficial.

In this paper, we develop a new third-order WENO-type scheme (called *ES*WENO) with the modified weight functions, which is suitable for linear wave equations and hyperbolic systems with discontinuous solutions, and prove that the new scheme is *E*nergy *S*table, i.e. stable in an L_2-energy norm. By construction, the ESWENO scheme satisfies *nonlinear* SBP and positive semidefiniteness conditions at each instant in time, which provide energy stability. Thus, L_2 strict stability is attained without the need for a TVB flux reconstruction, or a large-time-step constraint. Despite the SBP stencil constraint, the new ESWENO scheme still retains the underlying WENO characteristics. Indeed, numerical experiments demonstrate that the ESWENO scheme delivers stable essentially non-oscillatory solutions for problems with strong discontinuities.

This paper is organized as follows. In Section 2, an energy estimate for the continuous singular perturbed wave equation is obtained, followed by an energy estimate for the corresponding discrete problem. In Section 3, we present new weight functions and show that the dissipation operator of the conventional third-order WENO scheme is not positive semidefinite, thus indicating that the scheme may become locally unstable if strong discontinuities or unresolved features are present in the domain. In Section 4, we present the third-order ESWENO scheme and prove that the new scheme is stable in the energy norm, third-order accurate for smooth solutions including local smooth extrema, and conservative. Furthermore, based on the truncation error analysis, we show how to choose the tuning parameters of the weight functions to significantly improve the dissipation properties of the ESWENO scheme. In Section 5, we extend the scalar ESWENO scheme to hyperbolic systems and obtain an energy estimate for the characteristic form of the hyperbolic system of equations, while a similar estimate is not available if the system is discretized in the component-wise fashion. In Section 6, we present numerical experiments that corroborate our theoretical results. We summarize and draw conclusions in Section 7.

2. Energy estimates

Semi-discrete summation-by-parts (SBP) operators are constructed to explicitly satisfy an L_2-energy estimate. That is, the semi-discrete operator "mimics" the continuous operator in terms of the energy of the system. We begin by presenting a derivation of the energy estimate for the continuous system, followed by a derivation of the mimetic SBP semi-discrete operator.

2.1. The continuous problem

Consider a linear, scalar wave equation with periodic boundary conditions

$$\begin{aligned} &\frac{\partial u}{\partial t}+\frac{\partial f}{\partial x}=0, \quad f=au, \quad t\geqslant 0, \quad 0\leqslant x\leqslant 1,\\ &u(0,x)=u_0(x),\\ &u(t,0)=u(t,1), \end{aligned} \tag{1}$$

where a is a constant, and $u_0(x)$ is a bounded piecewise continuous function. Without loss of generality, we assume that $a \geqslant 0$.

Along with Eq. (1), we also consider the following singular perturbed wave equation which is subject to periodic boundary conditions

$$\begin{aligned} &\frac{\partial u}{\partial t}+\frac{\partial f}{\partial x}=\frac{\partial}{\partial x}\left(B\frac{\partial u}{\partial x}\right), \quad f=au, \quad t\geqslant 0, \quad 0\leqslant x\leqslant 1,\\ &u(0,x)=u_0(x), \end{aligned} \tag{2}$$

where B is a *nonlinear* positive semidefinite differential operator that depends only on u and its derivatives, i.e., $(v,Bv)=\int_0^1 vBvdx\geqslant 0$ for all sufficiently smooth functions $v(x)$ that satisfy the boundary conditions. The right-hand side of Eq. (2) can be interpreted as an artificial dissipation term for a finite difference scheme approximating Eq. (1).

To obtain an energy estimate, Eq. (2) is multiplied by u and integrated over the entire domain, which yields

$$\frac{1}{2}\frac{d}{dt}\|u\|_{l_2}^2+\frac{1}{2}au^2\Big|_0^1=uBu_x|_0^1-\int_0^1 u_xBu_xdx, \tag{3}$$

where $\|\cdot\|_{l_2}$ is the continuous l_2 norm. By taking into account that the boundary conditions are periodic and B depends only on u and its derivatives, the second term on the left-hand side and the first term on the right-hand side of Eq. (3) vanish, and the following energy estimate can be obtained

$$\frac{d}{dt}\|u\|_{l_2}^2=-2\int_0^1 u_xBu_xdx\leqslant 0. \tag{4}$$

Because B is a positive semidefinite differential operator, the right-hand side of Eq. (4) is nonpositive, thus providing the required dissipation property. It should be emphasized that in the above derivation, no additional assumptions have been made about B other than its positive semidefiniteness and that the operator B depends only on u and its derivatives, which makes Eq. (2) nonlinear.

2.2. The discrete problem

The energy estimate derivation for Eq. (2) relies on two properties of the continuous operator. First, the derivative operator $\frac{\partial f}{\partial x}$ must satisfy the integration-by-parts (IBP) property, i.e., $(v,f_x)=-(v_x,f)$ (for the periodic case). Second, the operator B must be positive semidefinite, i.e. $(v,Bv)=\int_0^1 vBvdx\geqslant 0$. In the present analysis, a stable, semi-discrete, third-order finite difference scheme for Eq. (1) is constructed by approximating f_x as a sum of two terms. The first term mimics the IBP property, while the second mimics the semidefiniteness of the operator B. This scheme is presented next.

Define a uniform grid $x_j=j\Delta x, j=\overline{0,J}$, with $\Delta x=1/J$. On that grid, define a flux $\bar{\mathbf{f}}=a\bar{\mathbf{u}}$ and its derivative $\bar{\mathbf{f}}_x=a\bar{\mathbf{u}}_x$, where $\bar{\mathbf{u}}=[u(x_0,t),\ldots,u(x_J,t)]^T$ and $\bar{\mathbf{u}}_x=[u_x(x_0,t),\ldots,u_x(x_J,t)]^T$ are projections of the continuous solution and its derivative onto the computational grid. Finally, define an approximation for the first-order derivative term in Eq. (1) as follows:

$$\frac{\partial\bar{\mathbf{f}}}{\partial x}=(D_c+D_a)\bar{\mathbf{f}}+O(\Delta x^{2p-1}). \tag{5}$$

The matrix D_c is a nonlinear central finite difference operator given by

$$\begin{aligned} &D_c=P^{-1}Q\ ;\ \bar{\mathbf{f}}_x-P^{-1}Q\bar{\mathbf{f}}=O(\Delta x^{2p}),\\ &P=\Delta xI\ ;\ Q+Q^T=0, \end{aligned} \tag{6}$$

where I is a $(J+1)\times(J+1)$ identity matrix. Note that the approximation (6) satisfies the SBP rule

$$(\mathbf{u},D_c\mathbf{v})_P=-(D_c\mathbf{u},\mathbf{v})_P \tag{7}$$

with $(\mathbf{u},\mathbf{v})_P=\mathbf{u}^TP\mathbf{v}$. Thus, the first mimetic relationship between the continuous and discrete equations is satisfied by D_c; i.e. *IBP* $\rightarrow$ *SBP*. (The relation $P=\Delta xI$ is valid only for the periodic case. Alterations in P result for the nonperiodic case, but this generality is outside the scope of the current work.)

The matrix D_a is a nonlinear finite difference artificial dissipation operator which mimics its continuous counterpart $\frac{\partial}{\partial x}\left(B\frac{\partial}{\partial x}\right)$. It is given by

$$D_a=P^{-1}D_1^TSD_1\ ;\ P^{-1}D_1^TSD_1\bar{\mathbf{u}}=O(\Delta x^{2p-1})\ ;\ \mathbf{v}^T(S+S^T)\mathbf{v}\geqslant 0, \tag{8}$$

where P is the same positive definite matrix used for the approximation of the first-order derivative term in Eq. (6), $\mathbf{v}$ is an arbitrary real-valued vector of length $(J+1)$, and D_1 and D_1^T are two-point difference operators given by

$$D_1=\begin{bmatrix} \ddots & & 0\\ -1 & 1 & \\ 0 & & \ddots \end{bmatrix},\quad D_1^T=\begin{bmatrix} \ddots & & 0\\ 1 & -1 & \\ 0 & & \ddots \end{bmatrix}.$$

Eq. (8) requires that the matrix S must be positive semidefinite, and that the nonlinear artificial dissipation term should be zero to the design order of the scheme (at least in regions where the solution of the differential problem (1) is sufficiently smooth).

Using the SBP operators given by Eqs. (6) and (8), (1) is discretized as follows:

$$\frac{\partial \mathbf{u}}{\partial t} + P^{-1} Q \mathbf{f} = -P^{-1} D_1^T S D_1 \mathbf{f}, \tag{9}$$

where $\mathbf{f} = a\mathbf{u}$ and $\mathbf{u} = [u_0(t), u_1(t), \ldots, u_J(t),]^T$ is the discrete approximation of the solution u of Eq. (1), Q and S are nonlinear matrices, i.e., $Q = Q(\mathbf{u})$ and $S = S(\mathbf{u})$. To show that the above finite difference scheme is stable, the energy method is used. Multiplying Eq. (9) with $\mathbf{u}^T P$ yields

$$\frac{1}{2}\frac{d}{dt}\|\mathbf{u}\|_P^2 + a\mathbf{u}^T Q \mathbf{u} = -a(D_1\mathbf{u})^T S D_1 \mathbf{u}, \tag{10}$$

where $\|\cdot\|_P$ is the P norm, i.e., $\|\mathbf{u}\|_P^2 = \mathbf{u}^T P \mathbf{u}$. Adding Eq. (10) to its transpose, we have

$$\frac{d}{dt}\|\mathbf{u}\|_P^2 + a\mathbf{u}^T (Q + Q^T)\mathbf{u} = -a(D_1\mathbf{u})^T (S + S^T) D_1 \mathbf{u}. \tag{11}$$

Taking into account that the boundary conditions are periodic and Q is fully skew-symmetric, the second term on the left-hand side vanishes, and the energy estimate becomes

$$\frac{d}{dt}\|\mathbf{u}\|_P^2 = -a(D_1\mathbf{u})^T (S + S^T) D_1 \mathbf{u} \leqslant 0. \tag{12}$$

The right-hand side of Eq. (12) is nonpositive, because the matrix S is positive semidefinite and $a \geqslant 0$, thus providing stability of the finite difference scheme Eq. (9). This result can be summarized in the following theorem:

Theorem 1. *The approximation (9) of the problem (1) is stable if Eqs. (6) and (8) hold.*

Remark 1. Despite the fact that the initial boundary value problem (1) is linear, the finite difference scheme (9) constructed for approximation of Eq. (1) is nonlinear, because it is assumed that the matrices Q and S (and in principle P) depend on the discrete solution $\mathbf{u}$.

Remark 2. The only constraints imposed on the matrices Q and S are skew-symmetry of the former and positive semidefiniteness of the later. No other assumptions have been made about a specific form of the matrices Q and S to guarantee the stability of the finite difference scheme (9).

Remark 3. The discrete operators defined by Eqs. (5)–(8) are symbolically identical to those used for conventional SBP operators (see [20–26]). What is new, however, is the fact that the matrices Q and S depend on $\mathbf{u}$.

3. Third-order WENO Scheme

3.1. Definitions

The conventional WENO scheme developed in [3] for the scalar 1-D wave Eq. (1) with $a \geqslant 0$ is given by

$$\frac{du_j}{dt} + \frac{f^{\mathrm{W}}_{j+\frac{1}{2}} - f^{\mathrm{W}}_{j-\frac{1}{2}}}{\Delta x} = 0, \tag{13}$$

where $f^{\mathrm{W}}_{j+\frac{1}{2}}$ is the third-order WENO flux which is

$$f^{\mathrm{W}}_{j+\frac{1}{2}} = w^0_{j+1/2} f^{(0)}_{j+1/2} + w^1_{j+1/2} f^{(1)}_{j+1/2}, \tag{14}$$

where w^0 and w^1 are weight functions assigned to two stencils $\{x_j, x_{j+1}\}$ and $\{x_{j-1}, x_j\}$, respectively. The second-order fluxes $f^{(r)}_{j+1/2}$ in Eq. (14) are defined on these two different stencils as follows:

$$\begin{aligned} f^{(0)}_{j+1/2} &= \frac{1}{2} f(u_j) + \frac{1}{2} f(u_{j+1}), \\ f^{(1)}_{j+1/2} &= -\frac{1}{2} f(u_{j-1}) + \frac{3}{2} f(u_j). \end{aligned} \tag{15}$$

In the present analysis, if the flux in Eq. (1) does not possess the property $f'(u) = a \geqslant 0$, then the global Lax–Friedrichs flux splitting is used

$$f^{\pm}(u) = \frac{1}{2}(f(u) \pm \lambda_{\max} u), \tag{16}$$

where $\lambda_{\max}$ is a constant that satisfies the following constraint

$$\lambda_{\max} \geqslant |a|. \tag{17}$$

The second-order stencils for $f^{-}_{j+\frac{1}{2}}$ are a mirror image of the stencils used for $f^{+}_{j+\frac{1}{2}}$ with respect to a point $j+\frac{1}{2}$.

The classical weight functions proposed by Jiang and Shu in [3] are given by

$$w^r_{j+\frac{1}{2}} = \frac{\alpha_r}{\alpha_0+\alpha_1}, \quad r = 0,1 \tag{18}$$

with

$$\alpha_r = \frac{d_r}{(\epsilon+\beta_r)^2}, \tag{19}$$

$$\begin{aligned} &d_0 = \tfrac{2}{3}, \quad d_1 = \tfrac{1}{3}, \\ &\beta_0 = (u_{j+1}-u_j)^2, \quad \beta_1 = (u_j - u_{j-1})^2, \end{aligned} \tag{20}$$

where the parameter ϵ in Eq. (19) is usually set to be 10^{-6}, as recommended in [3].

It is well known that the standard weight functions (18)–(20) make the corresponding WENO scheme too dissipative [5,27,28]. Furthermore, as will be shown in Section 4.2, the conventional third-order WENO scheme presented above may locally degenerate to second order near local extrema. These properties of the classical weight functions indicate that new weight functions are needed to recover the design order of convergence near the critical points.

We now present the new weight functions for the third-order ESWENO scheme. Note that these weights can also be used with the conventional third-order WENO scheme. Similar to the classical weights, the new weight functions are given by the formula (18), whereas the functions α_0 and α_1 are different from their classical counterparts and defined as

$$\alpha_r = d_r\left(1+\frac{\tau}{\epsilon+\beta_r}\right), \quad r = 0,1, \tag{21}$$

$$\tau = (u_{j+1} - 2u_j + u_{j-1})^2, \tag{22}$$

where ϵ is a small positive parameter that may depend on Δx. As will be shown in Sections 4.2 and 6, the new weight functions ((18) and (20)–(22)) provide consistency of the third-order ESWENO scheme and much faster convergence of this nonlinear scheme to the corresponding third-order underlying linear scheme, while preserving the ENO stencil biasing property near strong discontinuities.

Note that the new weights given by ((18) and (20)–(22)) are similar to those proposed in [27] for the fifth-order WENO scheme. The key difference between the new weights and those developed in [27] is the choice of the function τ in Eq. (21). To our knowledge, no weight functions similar to those developed in [27] for the fifth-order WENO scheme are currently available for the third-order WENO scheme. Furthermore, the same approach used to build τ for the the fifth-order WENO scheme in [27], i.e., $\tau = |\beta_0 - \beta_1|$, is not directly applicable to the third-order case, because $|\beta_0 - \beta_1| = O(\Delta x^3)$, thus leading to $w^r_{j+\frac{1}{2}} = d_r + O(\Delta x)$ which does not provide consistency of the third-order WENO and ESWENO schemes.

The new weight functions presented above possess the following two properties:

$$0 \leqslant w^r_{j+\frac{1}{2}} \leqslant 1, \quad w^0_{j+\frac{1}{2}} + w^1_{j+\frac{1}{2}} = 1 \text{ for } r = 0,1, \quad j = \overline{0,J}, \tag{23}$$

$$w^r_{j+\frac{1}{2}} = d_r + O(\Delta x^2) \text{ for } \quad r = 0,1. \tag{24}$$

Eq. (23) is valid for any vector $\mathbf{u}$, whereas Eq. (24) holds only if the solution is sufficiently smooth and some constraints are imposed on the parameter ϵ in Eq. (21), which will be discussed in Section 4.2.

3.2. Stability analysis

Before constructing a new Energy Stable WENO (ESWENO) scheme, we first show that the conventional third-order WENO scheme developed in [3] can be represented in the form of Eq. (9) with appropriate choices for the matrices P, Q, and S. Note, however, that the matrix S of the WENO scheme does not, satisfy all the sufficient conditions (8). Thus, it is not immediately evident how to form an energy estimate for this scheme.

To show this, we begin by defining the third-order WENO derivative matrix

$$D_W\mathbf{f} = \frac{f^W_{j+\frac{1}{2}} - f^W_{j-\frac{1}{2}}}{\Delta x}. \tag{25}$$

Substituting Eqs. (14) and (15) into (25) (and without loss of generality assuming $f'(u) = a \geqslant 0$) yields the periodic pentadiagonal matrix D_W,

$$D_W = Penta[d_{j-2}, d_{j-1}, d_j, d_{j+1}, d_{j+2}]$$

with entries

$$\begin{bmatrix} d_{j-2} \\ d_{j-1} \\ d_j \\ d_{j+1} \\ d_{j+2} \end{bmatrix}^T = \frac{1}{2\Delta x} \begin{bmatrix} w^1_{j-\frac{1}{2}} \\ -3w^1_{j-\frac{1}{2}} - w^1_{j+\frac{1}{2}} - w^0_{j-\frac{1}{2}} \\ 3w^1_{j+\frac{1}{2}} - w^0_{j-\frac{1}{2}} + w^0_{j+\frac{1}{2}} \\ w^0_{j+\frac{1}{2}} \\ 0 \end{bmatrix}^T. \tag{26}$$

If the symmetric part of D_W is positive semidefinite for all values of the parameters w^k_j (thereby emulating the conditions of Theorem 1), then stability immediately follows. To represent D_W in the form of Eq. (9), we decompose D_W into its symmetric and skew-symmetric components

$$D_W = \frac{1}{2}[D_W - (D_W)^T] + \frac{1}{2}[D_W + (D_W)^T] = D^{skew}_W + D^{sym}_W. \tag{27}$$

Equating the skew-symmetric and symmetric components of D_W with the equivalent terms from Eq. (9) yields

$$\begin{aligned} D^{skew}_W &= P^{-1}Q = Penta[q_{j-2}, q_{j-1}, q_j, q_{j+1}, q_{j+2}], \\ D^{sym}_W &= P^{-1}D_1^T S^{\mathrm{W}} D_1 = Penta[r_{j-2}, r_{j-1}, r_j, r_{j+1}, r_{j+2}] \end{aligned} \tag{28}$$

with

$$\begin{bmatrix} q_{j-2} \\ q_{j-1} \\ q_j \\ q_{j+1} \\ q_{j+2} \end{bmatrix}^T = \frac{1}{4\Delta x} \begin{bmatrix} w^1_{j-\frac{1}{2}} \\ -3w^1_{j-\frac{1}{2}} - w^1_{j+\frac{1}{2}} - 2w^0_{j-\frac{1}{2}} \\ 0 \\ 3w^1_{j+\frac{1}{2}} + w^1_{j+\frac{3}{2}} + 2w^0_{j+\frac{1}{2}} \\ -w^1_{j+\frac{3}{2}} \end{bmatrix}^T \tag{29}$$

and

$$\begin{bmatrix} r_{j-2} \\ r_{j-1} \\ r_j \\ r_{j+1} \\ r_{j+2} \end{bmatrix}^T = \frac{1}{4\Delta x} \begin{bmatrix} w^1_{j-\frac{1}{2}} \\ -3w^1_{j-\frac{1}{2}} - w^1_{j+\frac{1}{2}} \\ 2\left(3w^1_{j+\frac{1}{2}} - w^0_{j-\frac{1}{2}} + w^0_{j+\frac{1}{2}}\right) \\ -3w^1_{j+\frac{1}{2}} - w^1_{j+\frac{3}{2}} \\ w^1_{j+\frac{3}{2}} \end{bmatrix}^T. \tag{30}$$

The pentadiagonal matrix Q does not contribute to the P-norm of the energy, because it is entirely skew-symmetric. Inspection of Eq. (29) immediately reveals that the matrices P and Q are given by

$$P = \Delta x I \quad ; \quad Q = PD^{skew}_W. \tag{31}$$

The diagonal P matrix in Eq. (31) is symmetric positive definite, thus making it suitable as a norm.

Let us show that the symmetric part of D_W is not positive semidefinite. Lengthy manipulations of the expression

$$D^{sym}_W = P^{-1}D_1^T S^{\mathrm{W}} D_1 = Penta[r_{j-2}, r_{j-1}, r_j, r_{j+1}, r_{j+2}],$$

reveal that periodic matrix S^{W} derived from the conventional third-order WENO scheme (13)–(15), (18)–(20) is tridiagonal and given by the form

$$S^{\mathrm{W}} = Tri\left[-\frac{1}{4}w^1_{j-\frac{1}{2}}, \frac{1}{2}w^1_{j-\frac{1}{2}}, -\frac{1}{4}w^1_{j+\frac{1}{2}}\right]. \tag{32}$$

Given Eq. (32), it is still not apparent whether or not the symmetric part of S^{W} is positive semidefinite, the sufficient condition for stability of the discretization (9). Further tedious manipulations reveal that the tridiagonal matrix S^{W} in the WENO artificial dissipation operator can be written as

$$S^{\mathrm{W}} = S^{\mathrm{W}}_1 + D_1^T S^{\mathrm{W}}_2 D_1, \tag{33}$$

where S^{W}_1 and S^{W}_2 are the following diagonal matrices:

$$\begin{aligned} s^{\mathrm{w}}_{1_{jj}} &= -\frac{1}{4}\left(w^1_{j+\frac{1}{2}} - w^1_{j-\frac{1}{2}}\right), \\ s^{\mathrm{w}}_{2_{jj}} &= \frac{1}{4}w^1_{j-\frac{1}{2}}. \end{aligned} \tag{34}$$

From Eq. (34) it immediately follows that S_W in Eq. (32) is not positive semidefinite and therefore does not satisfy the conditions of Theorem 1. Indeed, the diagonal matrix S_2^W is positive semidefinite because $w^1_{j-\frac{1}{2}} \geqslant 0$ for all j, while the diagonal matrix S_1^W given by Eq. (34) is not positive semidefinite, because $s^w_{1_{jj}}$ can be either positive or negative. As a result, the third-order WENO scheme of Jiang and Shu does not provide the energy estimate obtained in Section 2. Furthermore, near strong discontinuities or unresolved features, $s^w_{1_{jj}}$ may become $O(1)$, thus shifting the eigenvalues of the WENO artificial dissipation operator $-P^{-1}D_1^T S^W D_1$ to the right half-plane. Because Theorem 1 provides only the sufficient condition for stability, no conclusion can be made about stability of the conventional WENO scheme for Eq. (1) with a discontinuous initial condition. Note that in [3], the stability of the WENO scheme has been proven only for sufficiently smooth solutions.

4. Third-order Energy Stable WENO scheme for the scalar wave equation

We now construct the operators P, Q, and S in Eq. (9) such that all the conditions of Theorem 1 are met. As has been shown in the foregoing section, the operators P and Q defined by Eq. (31) satisfy the conditions of Theorem 1 and can be directly incorporated into the new ESWENO scheme. The only condition that has not been met is positive semidefiniteness of the matrix S in the artificial dissipation operator D_a. We propose the following symmetric matrix S in Eq. (9), which possesses the required properties (8):

$$S = S_1 + D_1^T S_2 D_1, \tag{35}$$

where S_1 and S_2 are the following diagonal matrices:

$$\begin{aligned} s_{1_{jj}} &= \mu_j - \frac{1}{8}\left(w^1_{j+\frac{1}{2}} - w^1_{j-\frac{1}{2}}\right), \\ s_{2_{jj}} &= \frac{1}{4} w^1_{j-\frac{1}{2}}, \end{aligned} \tag{36}$$

where

$$\mu_j = \frac{1}{8}\sqrt{\left(w^1_{j+\frac{1}{2}} - w^1_{j-\frac{1}{2}}\right)^2 + \delta^2} \tag{37}$$

and δ is a small positive parameter which may depend on Δx. Possible ways how one can chose the parameter δ are discussed in Sections 4.2 and 4.3. Note that that parameter δ in Eq. (37) has been introduced only to provide smoothness of μ_j which is a C^∞ function of $\mathbf{u}$, thus making it consistent with the smoothness of the weight functions.

The ESWENO scheme is given by Eq. (9) with P, Q, and S defined by Eqs. (31) and (35)–(37) and the weights ((18) and (20)–(22)). We will show next that the ESWENO scheme is: (1) stable in the energy norm, (2) third-order accurate, if the solution of Eq. (1) is sufficiently smooth and some constraints are imposed on ϵ and δ, and (3) conservative.

Remark 4. The third-order ESWENO scheme has a 5-point stencil which is as wide as the stencil of the conventional third-order WENO scheme.

4.1. Stability

Theorem 1 provides the sufficient conditions (6) and (8) for stability of the finite difference ESWENO scheme (9). Therefore, if the constraints (6) and (8) are met, then the proposed ESWENO scheme is stable in the energy norm. It can be easily shown that the matrices P and Q defined by Eq. (31) satisfy the conditions (6). Therefore, to prove the stability of the proposed ESWENO scheme, one only has to show that the real-valued, nonlinear operator S given by Eqs. (35)–(37), (18), (20)–(22) is positive semidefinite, i.e., $\mathbf{v}^T S \mathbf{v} = \mathbf{v}^T \left(\frac{S+S^T}{2}\right)\mathbf{v} \geqslant 0$ for all discrete real-valued vectors $\mathbf{v}$ of length $(J+1)$. Let us show that the matrix S possesses this property. Indeed, the diagonal matrix S_2 given by Eq. (36) is positive semidefinite, because $w^1_{j-\frac{1}{2}} \geqslant 0$ for all j. From the following inequality which holds for any weight function $w^1_{j+\frac{1}{2}}$ if $\delta > 0$:

$$\frac{1}{8}\sqrt{\left(w^1_{j+\frac{1}{2}} - w^1_{j-\frac{1}{2}}\right)^2 + \delta^2} - \frac{1}{8}\left(w^1_{j+\frac{1}{2}} - w^1_{j-\frac{1}{2}}\right) > 0,$$

it immediately follows that each diagonal element $s_{1_{jj}}$ is positive, thus providing positive definiteness of S_1. Hence, the symmetric matrix S given by Eq. (35) is positive definite. Note, however, that $D_1^T S D_1$ is positive semidefinite rather than positive definite, because for $\mathbf{v} = (1, \ldots, 1)^T$, we have $(D_1\mathbf{v})^T S D_1 \mathbf{v} = 0$. It should also be noted that the matrix S depends on the discrete solution $\mathbf{u}$ of Eq. (9) and is positive definite for any real-valued vector $\mathbf{u}$ regardless of whether $\mathbf{u}$ is continuous or discontinuous.

Remark 5. The parameter μ_j can be chosen in many different ways so that it provides the energy estimate and consistency. Among possible candidates for μ_j, there is at least one that requires no tuning parameters, which is given by

$$\mu_j = \frac{1}{8}\left(w^1_{j+\frac{1}{2}} - w^1_{j-\frac{1}{2}}\right). \tag{38}$$

Note, however, that this particular choice of μ_j defined by Eq. (38) results in that the additional artificial "dissipation" operator, $D_1^T diag[\mu_j - 1/2 s_{1jj}^w] D_1$, is not actually dissipative. Since our primary objective is to construct an artificial dissipation operator, the above nondissipative operator is not considered herein.

Remark 6. Only the property (23) has been used to prove the positive definiteness of the matrix S. This property does not depend on a particular form of the weight functions and remains valid for any weight functions that satisfy Eq. (23).

Remark 7. The energy estimate cannot be obtained if the weights are negative, because in this case, the matrix S is not positive semidefinite.

4.2. Consistency

As has been shown in [28] for the conventional fifth-order WENO scheme, the sufficient condition on the weight functions obtained in [3] is incomplete. The same conclusion can be drawn for the conventional third-order WENO scheme. Therefore, we first derive necessary and sufficient conditions on the weight functions, which guarantee that the conventional WENO scheme given by Eqs. (13)–(15) is third-order accurate.

Expanding Eq. (15) in a Taylor series, we have

$$\begin{aligned} f_{j\pm1/2}^{(0)} &= h(x_{j\pm1/2}) + \frac{1}{4} f_{xx}\Delta x^2 + \frac{1}{12} f_{xxx}\Delta x^3 + O(\Delta x^4), \\ f_{j\pm1/2}^{(1)} &= h(x_{j\pm1/2}) - \frac{1}{4} f_{xx}\Delta x^2 + \frac{1}{12} f_{xxx}\Delta x^3 + O(\Delta x^4), \end{aligned} \tag{39}$$

where $h(x)$ is the numerical flux function which is implicitly defined as

$$f(x) = \frac{1}{\Delta x}\int_{x-\frac{\Delta x}{2}}^{x+\frac{\Delta x}{2}} h(\eta)d\eta. \tag{40}$$

Approximating the first-order derivative f_x at x_j by using the third-order WENO operator yields

$$\frac{f_{j+1/2}^W - f_{j-1/2}^W}{\Delta x} = \frac{\sum_{r=0}^{1}\left(w_{j+1/2}^r f_{j+1/2}^{(r)} - w_{j-1/2}^r f_{j-1/2}^{(r)}\right)}{\Delta x}. \tag{41}$$

If the solution is sufficiently smooth in all candidate stencils, then the weights $w_{j+1/2}^r$ approach their preferred values d_r, and the WENO operator converges to the target linear operator which is third-order accurate, i.e.,

$$\left.\frac{\partial f}{\partial x}\right|_{x=x_j} = \frac{\sum_{r=0}^{1}\left(d_r f_{j+1/2}^{(r)} - d_r f_{j-1/2}^{(r)}\right)}{\Delta x} + O(\Delta x^3). \tag{42}$$

Subtracting Eq. (42) from Eq. (41) and taking into account Eq. (39) gives

$$\begin{aligned} &\frac{1}{\Delta x}\sum_{r=0}^{1}\left[\left(w_{j+1/2}^r - d_r\right)f_{j+1/2}^{(r)} - \left(w_{j-1/2}^r - d_r\right)f_{j-1/2}^{(r)}\right] \\ &= \frac{1}{\Delta x}\sum_{r=0}^{1}\left[\left(w_{j+1/2}^r - d_r\right)h(x_{j+1/2}) - \left(w_{j-1/2}^r - d_r\right)h(x_{j-1/2})\right] + \sum_{r=0}^{1}\Delta x c_{1r}\left[\left(w_{j+1/2}^r - d_r\right) - \left(w_{j-1/2}^r - d_r\right)\right] \\ &+ \sum_{r=0}^{1}\Delta x^2 c_{2r}\left[\left(w_{j+1/2}^r - d_r\right) - \left(w_{j-1/2}^r - d_r\right)\right] + O(\Delta x^3), \end{aligned} \tag{43}$$

where

$$\begin{aligned} c_{10} &= -c_{11} = \frac{1}{4} f_{xx}(x_j), \\ c_{20} &= c_{21} = \frac{1}{12} f_{xxx}(x_j). \end{aligned} \tag{44}$$

Eq. (43) leads to the following necessary and sufficient conditions that provide third-order convergence of the WENO scheme (13)–(15):

$$\begin{aligned} &\sum_{r=0}^{1}(w_{j\pm1/2}^r - d_r) = O(\Delta x^4), \\ &\sum_{r=0}^{1} c_{1r}[(w_{j+1/2}^r - d_r) - (w_{j-1/2}^r - d_r)] = O(\Delta x^2), \\ &\sum_{r=0}^{1} c_{2r}[(w_{j+1/2}^r - d_r) - (w_{j-1/2}^r - d_r)] = O(\Delta x), \end{aligned} \tag{45}$$

As follows from Eqs. (20) and (23), the first condition in Eq. (45) is always met. Taking into account the exact expressions for c_{20} and c_{21} given by Eqs. (44) and (20), (23), it can be easily shown that the last constraint in Eq. (45) is also satisfied automatically. To simplify the further analysis, the second constraint in Eq. (45) is replaced with the following sufficient condition:

$$w^r_{j+1/2} - d_r = O(\Delta x^2) \quad r = 0, 1, \tag{46}$$

which guarantees that the conventional third-order WENO scheme is design-order accurate. Note that Eq. (46) imposes a more sever constraint on the weights as compared with $w^r = d_r + O(\Delta x)$ which was obtained in [3].

We now prove that the same constraint (46) suffices to guarantee that the ESWENO scheme given by Eqs. (9), (31) and (35)–(37) is third-order accurate, if the parameter δ in Eq. (37) satisfies the following condition:

$$\delta = O(\Delta x^2), \tag{47}$$

where Δx is the grid spacing.

The P and Q operators of the ESWENO scheme are identical to those of the conventional third-order WENO scheme. Comparing Eqs. (33)–(37), one can see that the ESWENO scheme can be obtained from the WENO scheme of Jiang and Shu by adding the following additional artificial dissipation term:

$$[D_{\mathrm{ES}}\mathbf{u} - D_W\mathbf{u}]_j = \frac{\hat{e}_{j+\frac{1}{2}} - \hat{e}_{j-\frac{1}{2}}}{\Delta x}, \ \hat{e}_{j+\frac{1}{2}} = \left(\mu_{j+1} + \frac{w^1_{j+\frac{3}{2}} - w^1_{j+\frac{1}{2}}}{8}\right)(f_j - f_{j+1}), \tag{48}$$

where μ_j is defined by Eq. (37) and D_{ES} and D_W are the ESWENO and WENO operators, respectively. Assuming that Eqs. (46) and (47) hold, we have

$$\hat{e}_{j+\frac{1}{2}} = \left(\frac{1}{8}\sqrt{\left(w^1_{j+\frac{3}{2}} - d_1 + d_1 - w^1_{j+\frac{1}{2}}\right)^2 + \delta^2} + \frac{w^1_{j+\frac{3}{2}} - d_1 + d_1 - w^1_{j+\frac{1}{2}}}{8}\right)(f_j - f_{j+1}) = O(\Delta x^2)(f_j - f_{j+1}). \tag{49}$$

Substituting Eq. (49) in Eq. (48) yields

$$\frac{\hat{e}_{j+\frac{1}{2}} - \hat{e}_{j-\frac{1}{2}}}{\Delta x} = O(\Delta x^2)\frac{f_{i+1} - 2f_i + f_{i-1}}{\Delta x} = O(\Delta x^3). \tag{50}$$

The above equation has been derived using $f_{j+1} - 2f_j + f_{j-1} = O(\Delta x^2)$. From Eq. (50) it immediately follows that the conditions (46) and (47) are sufficient to provide third-order accuracy of the ESWENO scheme.

Remark 8. δ is a user-defined parameter. Therefore, the constraint (47) can always be satisfied.

To prove consistency of the third-order WENO and ESWENO schemes, we need only show that the new weight functions (18) and (20)–(22) satisfy the sufficient condition (46). Let us show that this statement remains true even for smooth solutions with any number of vanishing derivatives, if the following constraint is imposed on the parameter ϵ in Eq. (21):

$$\epsilon \geqslant O(\Delta x^2). \tag{51}$$

Indeed, expanding the smoothness indicators β_r and the function τ in Eqs. (20) and (22) in a Taylor series about x_j, we have

$$\begin{aligned} \beta_0 &= (\bar{u}_x)^2\Delta x^2 + \bar{u}_x\bar{u}_{xx}\Delta x^3 + \left(\tfrac{1}{4}(\bar{u}_{xx})^2 + \tfrac{1}{3}\bar{u}_x\bar{u}_{xxx}\right)\Delta x^4 + O(\Delta x^4), \\ \beta_1 &= (\bar{u}_x)^2\Delta x^2 - \bar{u}_x\bar{u}_{xx}\Delta x^3 + \left(\tfrac{1}{4}(\bar{u}_{xx})^2 + \tfrac{1}{3}\bar{u}_x\bar{u}_{xxx}\right)\Delta x^4 + O(\Delta x^4), \end{aligned} \tag{52}$$

$$\tau = (\bar{u}_{xx})^2\Delta x^4 + O(\Delta x^5), \tag{53}$$

where $\bar{u}_x = \bar{u}_x(x_j), \bar{u}_{xx} = \bar{u}_{xx}(x_j)$, and $\bar{u}_{xxx} = \bar{u}_{xxx}(x_j)$ are projections of the continuous solution and its derivatives on the computational grid. For sufficiently smooth solutions with arbitrary number n_{vd} of vanishing derivatives (i.e., $u_x(x_c) = \cdots = u_x^{(n_{vd})}(x_c) = 0, u_x^{(n_{vd}+1)}(x_c) \neq 0$), the following inequalities hold asymptotically:

$$\epsilon \geqslant O(\Delta x^2) \gg O(\Delta x^4) \geqslant \tau. \tag{54}$$

As a result, $\tau/(\epsilon + \beta_r)$ can be recast as follows:

$$\frac{\tau}{\epsilon + \beta_r} \leqslant \frac{O(\Delta x^4)}{O(\Delta x^2)} = O(\Delta x^2). \tag{55}$$

Substituting Eq. (55) into Eq. (18) and subtracting d_r yields

$$w^r - d_r = \frac{d_r + \frac{d_r\tau}{\epsilon+\beta_r}}{1 + \frac{d_0\tau}{\epsilon+\beta_0} + \frac{d_1\tau}{\epsilon+\beta_1}} - d_r \leqslant \frac{O(\Delta x^2)}{1 + O(\Delta x^2)} = O(\Delta x^2). \tag{56}$$

Note that no assumptions about the number of vanishing derivatives have been used to derive the above equation. Consequently, the new weight functions satisfy the sufficient condition (46) for smooth solutions with arbitrary number of vanishing derivatives, thus providing consistency of the third-order WENO and ESWENO schemes.

If the constraint (51) is not met, then the order of the WENO and ESWENO schemes with the new weights (18) and (20)–(22) may locally deteriorate from 3 to 2. This deterioration in accuracy occurs near local extrema. Let x_c be a local extremum such that $\bar{u}_x(x_c) = 0$ and $\bar{u}_{xx}(x_c) \neq 0$. Assuming that $\epsilon = 0$ and using Eqs. (52) and (53), the expression $\tau/(\epsilon + \beta_r)$ at $x = x_c$ can be evaluated as

$$\frac{\tau}{\epsilon + \beta_r} = \frac{O(\Delta x^4)}{O(\Delta x^4)} = O(1), \tag{57}$$

thus leading to $w^r = O(1)$. The result is that both the third-order WENO and ESWENO schemes locally degenerate to second order. Note, however, that if the parameter ϵ satisfies the constraint (51), then the WENO and ESWENO schemes are third-order accurate for smooth solutions with any number of vanishing derivatives.

Near smooth extrema, the conventional third-order WENO scheme locally exhibits only a second-order convergence rate even on moderate grids that are widely used in practical applications. To demonstrate this, substitute Eq. (52) into the conventional weight function $w^0_{j+\frac{1}{2}}$ given by Eqs. (18)–(20) to obtain the relation

$$w^0_{j+\frac{1}{2}} = \frac{d_0}{d_0 + d_1\left[\frac{\epsilon/\Delta x^2 + \bar{u}_x^2 + \bar{u}_x\bar{u}_{xx}\Delta x + O(\Delta x^2)}{\epsilon/\Delta x^2 + \bar{u}_x^2 - \bar{u}_x\bar{u}_{xx}\Delta x + O(\Delta x^2)}\right]^2}. \tag{58}$$

For a given Δx, exceptional conditions occur in Eq. (58) if either $\epsilon/\Delta x^2 + \bar{u}_x^2 + \bar{u}_x\bar{u}_{xx}\Delta x = 0$ or $\epsilon/\Delta x^2 + \bar{u}_x^2 - \bar{u}_x\bar{u}_{xx}\Delta x = 0$ is satisfied near a local extremum of the continuous solution (e.g., where $\bar{u}_x$ decreases and passes through 0 and $\bar{u}_{xx} = O(1)$). The existence of such a zero is assured on a sufficiently coarse grid for $|u_{xx}| \geqslant \frac{2\sqrt{\epsilon}}{\Delta x^2}$, given that either relation is a quadratic equation in the variable $\bar{u}_x$. Next, without loss of generality, consider the point $x_j = x^*$ such that $\epsilon/\Delta x^2 + \bar{u}_x^2 + \bar{u}_x\bar{u}_{xx}\Delta x = 0$. Furthermore, assume that ϵ satisfies $\epsilon \leqslant O(\Delta x^3)$. With these assumptions, Eq. (58) can be recast in the following form:

$$w^0_{j+\frac{1}{2}} = \frac{d_0}{d_0 + d_1\left[\frac{O(\Delta x^2)}{2\epsilon/\Delta x^2 + 2\bar{u}_x^2 + O(\Delta x^2)}\right]^2} = \frac{d_0}{d_0 + O(\Delta x)} = 1 + O(\Delta x). \tag{59}$$

From Eq. (59), it follows that $w^0_{j+1/2} \neq d_0$ and the conventional WENO scheme locally degenerates to second order, if the grid spacing is of the order of $O(\epsilon^{1/3})$. For $\epsilon = 10^{-6}$, $\Delta x = O(\epsilon^{1/3}) = O(10^{-2})$ which indicates that this deterioration in accuracy may occur even on moderate grids.

4.3. How to choose parameters δ and ϵ

In contrast to the original WENO scheme [3] which has only one tuning parameter ϵ, the ESWENO scheme with the modified weight functions (18) and (20)–(22) and the additional artificial dissipation term (48) and (37) has two tuning parameters: δ and ϵ. In the foregoing section, we derived the constraints (47) and (51) that provide consistency of the third-order ESWENO scheme. These formulae give quite accurate estimates for δ and ϵ, but some ambiguity remains in how to choose coefficients in front of Δx^2 in Eqs. (47) and (51). This question will be addressed next.

To answer this question, we first consider how the new weights ((18) and (20)–(22) emulate the ENO stencil biasing strategy. Let $\bar{u}(x)$ be a piecewise smooth function on an interval $[x_{j-2}, x_{j+2}]$ such that the discontinuity is located at $x_d : x_j < x_d < x_{j+1}$. Then, the weight function $w^0_{j+1/2}$ can be evaluated as follows:

$$w^0_{j+\frac{1}{2}} = \frac{d_0\left(1 + \frac{O(1)}{\epsilon + O(1)}\right)}{1 + \frac{O(1)}{\epsilon + O(1)} + \frac{O(1)}{\epsilon + O(\Delta x^2)}} = O(1)(\epsilon + O(\Delta x^2)). \tag{60}$$

To emulate the ENO property near the strong discontinuity, the stencil $S_j = \{x_j, x_{j+1}\}$ has to be eliminated from the approximation by effectively nullifying $w^0_{j+1/2}$. As follows from Eq. (60), this property can be achieved if the following constraint is imposed on the parameter ϵ:

$$\epsilon \leqslant O(\Delta x^2). \tag{61}$$

Indeed, if the above constraint is satisfied, then $w^0_{j+1/2} = O(\Delta x^2)$. In addition, Eq. (61) provides that the weight $w^0_{j+1/2}$ has the same order as it would have if $\epsilon = 0$, thus minimizing the effect of the parameter ϵ on the numerical solution in the vicinity of the discontinuity. Comparing Eqs. (51) and (61), we can immediately conclude that

$$\epsilon = O(\Delta x^2). \tag{62}$$

Thus, if (47) and (62) are met then the ESWENO scheme is third-order accurate for smooth solutions with arbitrary number of vanishing derivatives and provides essentially non-oscillatory solutions for problems with strong discontinuities.

The original WENO scheme [3] is self similar, i.e., it is invariant when the spatial and time variables are scaled by the same factor. To make the ESWENO scheme self similar, the grid spacing Δx in Eqs. (47) and (51) is replaced with the grid spacing in the computational domain $\Delta\xi = 1/J$, where J is the total number of grid cells, thus leading to

$$\delta = O(\Delta\xi^2), \tag{63}$$

$$\epsilon = O(\Delta\xi^2). \tag{64}$$

The above formulae are fully consistent with Eqs. (47) and (62) and provide that WENO and ESWENO schemes with the new weights are invariant when the spatial and time variables are scaled by the same factor.

The parameters ϵ and δ in Eqs. (21) and (37) appear together with the β_r and $\left(w^1_{j+1/2} - w^1_{j-1/2}\right)^2$ terms, respectively, which gives us an indication that these terms should be scaled consistently. In regions where the solution is smooth, β_r approximates $u_\xi^2\Delta\xi^2$, while near unresolved features, β_r is of the order of u^2. The above consideration suggests that ϵ can be chosen as follows:

$$\epsilon = \max_{\xi\neq\xi_d}(\|u_0^2\|, \|(u_{0_\xi})^2\|)\Delta\xi^2, \tag{65}$$

where u_0 is the initial condition of Eq. (1), ξ_d is a set of points where the initial condition is discontinuous, and $\|\cdot\|$ is an appropriate norm. In all numerical experiments presented, we use the L_1 norm in Eq. (65). The scaling factor in Eq. (65) is a function of the initial condition, which can be readily calculated. Another advantage of Eq. (65) is that the parameter ϵ is evaluated only once, and the same value is used during the entire calculation, thus not increasing the CPU time.

As has been mentioned above, the parameter δ should be scaled consistently with $\left(w^1_{j+1/2} - w^1_{j-1/2}\right)^2$. Taking into account the fact that the weights are nondimensional quantities of the order of one, the scaling factor in front of the $\Delta\xi^2$ term in Eq. (63) is set to be 1, which results in the following formula for δ:

$$\delta = \Delta\xi^2. \tag{66}$$

Eqs. (65) and (66) eliminate the ambiguity in determining the parameters ϵ and δ, while providing the design order of convergence of the third-order WENO and ESWENO schemes and preserving their ENO properties.

4.4. Conservation

The Lax–Wendroff theorem [30] states that a convergent numerical approximation $u(x,t)$, computed with a consistent and *conservative* method, converges to a weak solution of the conservation law Eq. (1). Therefore, to accurately calculate the strength and speed of shock waves and contact discontinuities with finite mesh size, a difference operator should be discretely conservative. WENO schemes are used primarily to capture discontinuities while maintaining high-order accuracy in smooth portions of a solution. Thus, if the proposed ESWENO scheme is to be used for the same applications, it is essential that the scheme satisfies a discrete conservation condition.

For the continuous problem Eq. (1), integration over the spatial domain leads to

$$\frac{d}{dt}\int_0^1 u dx + f(t,1) - f(t,0) = 0. \tag{67}$$

The above equation shows that the total quantity of a conserved variable u in the domain changes only because of the flux through the domain boundaries. As has been shown in Section 4.2, the ESWENO scheme can be written in the semi-discrete conservative form (13) with the flux $f^{ES} = f^W + \hat{e}$, where f^W is the conventional WENO flux, and $\hat{e}$ is the additional dissipation flux term given by Eq. (48). From these equations it immediately follows that the numerical flux telescopes across the domain to the boundaries, thus mimicking the conservation property of the continuous problem and providing conservation at the discrete level.

5. ESWENO scheme for systems of equations

The ESWENO scheme constructed for the one-dimensional constant coefficient wave Eq. (1) can be extended to hyperbolic systems. There are two major approaches to generalization of scalar finite difference WENO-type schemes to systems of equations. The first approach is to discretize each equation in the system by using the scalar WENO-type scheme. In this case, the WENO reconstruction is done for each component of the vector separately. The second technique is based on the characteristic decomposition. The main idea of this approach is to transform the undivided differences to the local characteristic fields and perform the scalar WENO reconstruction for each component of the vector of the characteristic variables. The numerical flux calculated this way is then transformed back into the physical space. We will show in this section that the energy estimate can be obtained for the characteristic form of a hyperbolic system of constant coefficient equations, while it is not clear how to obtain a similar energy estimate when the system of equations is discretized in the component-wise fashion.

Let us consider a one-dimensional hyperbolic system of n equations with constant coefficients

$$\vec{u}_t + A\vec{u}_x = 0, \tag{68}$$

where $\vec{u}$ is a vector of length n, A is a constant $(n \times n)$ matrix which has n real eigenvalues: $\lambda_1 \leqslant \ldots \leqslant \lambda_n$, and a complete set of linearly independent eigenvectors: $\vec{r}_1, \ldots, \vec{r}_n$. By multiplying Eq. (68) by a matrix R composed of the eigenvectors of A, i.e., $R = (\vec{r}_1, \ldots, \vec{r}_n)$, and by introducing a vector of the characteristic variables $\vec{c} = R^{-1}\vec{u}$, the system of Eq. (68) can be rewritten in the following diagonal form:

$$\vec{c}_t + \Lambda\vec{c}_x = 0, \tag{69}$$

where $\Lambda = \mathrm{diag}(\lambda_1, \ldots, \lambda_n)$. The system of Eq. (69) is fully decoupled, so that each equation is a scalar constant coefficient wave equation of the form of Eq. (1). As in the scalar case, we assume that the systems of Eqs. (68) and (69) are subject to periodic boundary conditions.

In contrast to the scalar case where the wave velocity a is either positive or negative, the eigenvalues in the system of Eq. (69) may have different signs simultaneously. If this is the case, a flux splitting is used

$$\vec{f} = \vec{f}^{+} + \vec{f}^{-},$$

where the matrix $\frac{d\vec{f}(\vec{u})^{+}}{d\vec{u}}$ has only nonnegative eigenvalues, while the matrix $\frac{d\vec{f}(\vec{u})^{-}}{d\vec{u}}$ has only negative eigenvalues, where $\vec{f} = A\vec{u}$. For the characteristic form of the Eq. (69), the above splitting is simply equivalent to separating the equations with positive eigenvalues from those with negative eigenvalues. In the present analysis, the Lax–Friedrichs flux splitting given by Eq. (16) is used.

Both Eqs. (68) and (69) can be approximated by using the ESWENO scheme. However, as will be shown next, an energy estimate can be obtained only for the characteristic form of the governing Eq. (69), while similar estimate is not available for Eq. (68). Discretizing each equation in Eq. (69) by using the scalar ESWENO scheme (9), (31) and (35)–(37), the semi-discrete approximation of the characteristic form of the hyperbolic system of equations can be written as

$$\mathcal{C}_t + \mathcal{D}_c\mathcal{C} = -\mathcal{D}_a\mathcal{C}, \tag{70}$$

where $\mathcal{C} = [c_1^{(1)}, \ldots, c_J^{(1)}, \ldots, c_1^{(n)}, \ldots, c_J^{(n)}]^T$, $\mathcal{D}_c$ and $\mathcal{D}_a$ are block matrices defined as follows:

$$\begin{aligned}
\mathcal{D}_c &= \begin{bmatrix} \lambda_1 P^{-1} Q_1 & & 0 \\ & \ddots & \\ 0 & & \lambda_n P^{-1} Q_n \end{bmatrix}, \\
\mathcal{D}_a &= \begin{bmatrix} \lambda_1 P^{-1} D_1^T S_1 D_1 & & 0 \\ & \ddots & \\ 0 & & \lambda_n P^{-1} D_1^T S_n D_1 \end{bmatrix},
\end{aligned} \tag{71}$$

where P, Q_i, and $S_i, i = \overline{1,n}$ are $(J+1) \times (J+1)$ matrices which are given by Eqs. (31) and (35)–(37), respectively.

Hereafter in this section, without loss of generality, it is assumed that all eigenvalues of the matrix A are nonnegative, i.e.,

$$\lambda_n \geqslant \cdots \geqslant \lambda_1 \geqslant 0, \tag{72}$$

which is equivalent to using the flux splitting and considering only the positive flux $\vec{f}^{+} = \frac{|A|+A}{2}\vec{c}$, where $|\Lambda| = \mathrm{diag}(|\lambda_1|, \ldots, |\lambda_n|)$. For the flux $\vec{f}^{-}$, the ESWENO reconstruction and the corresponding matrices Q_i and S_i can be obtained as mirror images of those used for $\vec{f}^{+}$ with the respect to $x_{j+\frac{1}{2}}$. All results presented in this section for the positive ESWENO flux $\vec{f}^{+}$ remain valid for $\vec{f}^{-}$ as well.

The smoothness indicators used for calculation of Q_i and S_i are functions of $\mathbf{c}_i = [c_1^{(i)}, \ldots, c_J^{(i)}]^T$. In other words, for ith component of the vector of the characteristic variables, the smoothness indicators, which in the scalar case are defined by Eq. (20), are given by

$$\begin{aligned}
\beta_0 &= \left(c_{j+1}^{(i)} - c_j^{(i)}\right)^k, \\
\beta_1 &= \left(c_j^{(i)} - c_{j-1}^{(i)}\right)^k,
\end{aligned} \tag{73}$$

whereas the same formulae (18) and (20)–(22) are used for calculation of the weight functions. Hence,

$$Q_i \neq Q_l, \quad S_i \neq S_l \quad \text{if } i \neq l,$$

because the nonlinear operators Q_i and S_i depend on $\mathbf{c}_i = [c_1^{(i)}, \ldots, c_J^{(i)}]^T$, and therefore are different for each component of the vector of the characteristic variables.

We now prove that the ESWENO scheme given by Eqs. (70)–(72) is stable in the energy sense.

Theorem 2. *The approximation (70)–(72) with the matrices Q_i and $S_i, i = \overline{1,n}$ defined by Eqs. (31) and (35), respectively, is stable.*

Proof. An energy estimate for Eq. (69) can be obtained by employing the standard procedure used in the scalar case. Multiplying Eq. (70) with $\mathcal{C}^T\mathcal{P}$ leads to

$$\frac{1}{2}\frac{d}{dt}\|\mathcal{C}\|^2_{\mathcal{P}} + \mathcal{C}^T\mathcal{Q}\mathcal{C} = -\mathcal{C}^T\mathcal{S}\mathcal{C}, \tag{74}$$

where $\mathcal{P} = \mathrm{diag}(P,\ldots,P)$, $\|\mathcal{C}\|^2_{\mathcal{P}} = \sum_{i=1}^n \|\mathbf{c}_i\|^2_P$ and $\mathcal{Q}$ and $\mathcal{S}$ are the following block matrices:

$$\mathcal{Q} = \begin{bmatrix} \lambda_1 Q_1 & & 0 \\ & \ddots & \\ 0 & & \lambda_n Q_n \end{bmatrix}, \quad \mathcal{S} = \begin{bmatrix} \lambda_1 D_1^T S_1 D_1 & & 0 \\ & \ddots & \\ 0 & & \lambda_n D_1^T S_n D_1 \end{bmatrix}. \tag{75}$$

Adding Eq. (74) to its transpose, we have

$$\frac{d}{dt}\|\mathcal{C}\|^2_{\mathcal{P}} + \mathcal{C}^T(\mathcal{Q}+\mathcal{Q}^T)\mathcal{C} = -\mathcal{C}^T(\mathcal{S}+\mathcal{S}^T)\mathcal{C}. \tag{76}$$

Taking into account that the matrices $Q_i, i = \overline{1,n}$ are skew-symmetric and

$$\mathcal{Q}^T = \begin{bmatrix} \lambda_1 Q_1^T & & 0 \\ & \ddots & \\ 0 & & \lambda_n Q_n^T \end{bmatrix} = \begin{bmatrix} -\lambda_1 Q_1 & & 0 \\ & \ddots & \\ 0 & & -\lambda_n Q_n \end{bmatrix} = -\mathcal{Q}, \tag{77}$$

the second term on the left-hand side of Eq. (76) vanishes, and Eq. (76) can be recast as follows:

$$\frac{d}{dt}\|\mathcal{C}\|^2_{\mathcal{P}} = -\sum_{i=1}^n \lambda_i (D_1\mathbf{c}_i)^T (S_i + S_i^T) D_1\mathbf{c}_i \leqslant 0. \tag{78}$$

From Eq. (78), it follows that if Eq. (72) is valid and each matrix S_i, $i = \overline{1,n}$ is positive semidefinite, then the ESWENO scheme (70)–(72) is stable for systems of Eq. (69). □

Remark 9. Note that the standard approach used for proving Theorem 2 does not provide a similar energy estimate when the system of Eq. (68) is discretized by the ESWENO scheme in a component by component fashion. Indeed, discretizing Eq. (68) by using the ESWENO scheme yields

$$\mathcal{U}_t + \hat{\mathcal{D}}_{\mathrm{c}}\mathcal{U} = -\hat{\mathcal{D}}_{\mathrm{a}}\mathcal{U}, \tag{79}$$

where $\mathcal{U} = [u_1^{(1)},\ldots,u_j^{(1)},\ldots,u_1^{(n)},\ldots,u_j^{(n)}]^T$, $\hat{\mathcal{D}}_{\mathrm{c}}$ and $\hat{\mathcal{D}}_{\mathrm{a}}$ are defined as

$$\begin{aligned} \hat{\mathcal{D}}_{\mathrm{c}} &= \begin{bmatrix} a_{11}P^{-1}Q_1 & \ldots & a_{1n}P^{-1}Q_1 \\ \vdots & \ddots & \vdots \\ a_{n1}P^{-1}Q_n & \ldots & a_{nn}P^{-1}Q_n \end{bmatrix} \\ \hat{\mathcal{D}}_{\mathrm{a}} &= \begin{bmatrix} a_{11}P^{-1}D_1^T S_1 D_1 & \ldots & a_{1n}P^{-1}D_1^T S_1 D_1 \\ \vdots & \ddots & \vdots \\ a_{n1}P^{-1}D_1^T S_n D_1 & \ldots & a_{nn}P^{-1}D_1^T S_n D_1 \end{bmatrix}. \end{aligned} \tag{80}$$

Multiplying Eq. (79) by $\mathcal{U}^T\mathcal{P}$ and adding it to its transpose, we have

$$\frac{d}{dt}\|\mathcal{U}\|^2_{\mathcal{P}} + \mathcal{U}^T(\hat{\mathcal{Q}}+\hat{\mathcal{Q}}^T)\mathcal{U} = -(\mathcal{D}_1\mathcal{U})^T(\hat{\mathcal{S}}+\hat{\mathcal{S}}^T)\mathcal{D}_1\mathcal{U}, \tag{81}$$

where $\mathcal{D}_1 = \mathrm{diag}(D_1,\ldots,D_1)$, $\hat{\mathcal{Q}}$, $\hat{\mathcal{Q}}^T$, $\hat{\mathcal{S}}^T$, and $\hat{\mathcal{S}}^T$ are given by

$$\begin{aligned} \hat{\mathcal{Q}} &= \begin{bmatrix} a_{11}Q_1 & \ldots & a_{1n}Q_1 \\ \vdots & \ddots & \vdots \\ a_{n1}Q_n & \ldots & a_{nn}Q_n \end{bmatrix}, \quad \hat{\mathcal{Q}}^T = \begin{bmatrix} a_{11}Q_1^T & \ldots & a_{n1}Q_n^T \\ \vdots & \ddots & \vdots \\ a_{1n}Q_1^T & \ldots & a_{nn}Q_n^T \end{bmatrix}, \\ \hat{\mathcal{S}} &= \begin{bmatrix} a_{11}S_1 & \ldots & a_{1n}S_1 \\ \vdots & \ddots & \vdots \\ a_{n1}S_n & \ldots & a_{nn}S_n \end{bmatrix}, \quad \hat{\mathcal{S}}^T = \begin{bmatrix} a_{11}S_1^T & \ldots & a_{n1}S_n^T \\ \vdots & \ddots & \vdots \\ a_{1n}S_1^T & \ldots & a_{nn}S_n^T \end{bmatrix}. \end{aligned} \tag{82}$$

From the above equation, it immediately follows that although $Q_i = -Q_i^T$, for all $i = \overline{1,n}$, the matrix $\hat{\mathcal{Q}}$ is not skew-symmetric, thus making the second term on the left-hand side of Eq. (81) non-zero. Furthermore, the matrix $\hat{\mathcal{S}}+\hat{\mathcal{S}}^T$ is not positive semi-

Table 1
L_∞ error norms and their convergence rates obtained with the third-order ESWENO, WENO, and linear schemes.

J	Linear		ESWENO		WENO	
	$\|\bar{\mathbf{u}} - \mathbf{u}_h\|_{L_\infty}$	Rate	$\|\bar{\mathbf{u}} - \mathbf{u}_h\|_{L_\infty}$	Rate	$\|\bar{\mathbf{u}} - \mathbf{u}_h\|_{L_\infty}$	Rate
50	3.70e−1	–	3.87e−1	–	6.62e−1	–
100	1.49e−1	1.31	1.63e−1	1.25	4.70e−1	0.49
200	3.18e−2	2.23	3.69e−2	2.14	2.43e−1	0.95
400	4.47e−3	2.83	5.23e−3	2.82	9.38e−2	1.37
800	5.68e−4	2.97	6.37e−4	3.04	2.94e−2	1.67
1600	7.12e−5	3.00	7.58e−5	3.07	6.35e−3	2.21

definite because of the presence of a_{ij}. As a result, an energy estimate similar to one derived for the characteristic form of the hyperbolic system of Eq. (69) cannot be obtained when Eq. (68) are approximated in the component-wise fashion. A conclusion that can be drawn from this analysis is that to guarantee the stability of the ESWENO scheme for hyperbolic systems, the characteristic decomposition should be used in the ESWENO reconstruction. As has been shown numerically in [33], the component-wise high-order WENO reconstruction gives rise to spurious oscillations for problems with strong discontinuities, while the characteristic-wise WENO reconstruction allows one to obtain essentially non-oscillatory solutions, which corroborates our theoretical results.

6. Numerical results

In this section, we compare numerical results obtained with the third-order ESWENO and conventional WENO schemes. For all test problems considered, the CFL number is set to be 0.45 and the parameters ϵ and δ for the ESWENO scheme have been chosen in accordance with Eqs. (65) and (66). The parameter ϵ for the conventional third-order WENO scheme is set equal to 10^{-6}, as recommended in [3]. The time derivative is approximated using the third-order TVD Runge–Kutta method developed in [31].

6.1. Scalar linear wave equation

We begin by verifying that the ESWENO scheme is third-order accurate for smooth problems. To check this property, we consider Eq. (1) with $a = 0.5$ and the following initial condition:

$$u_0(x) = \begin{cases} [0.5 + 0.5\cos(w(x - x_c))]^4 & \text{if } |x - x_c| \leqslant \sigma, \\ 0 \quad \text{if } |x - x_c| > \sigma, \end{cases} \tag{83}$$

where w, x_c and σ are equal to 5π, 0.5, and 0.2, respectively. The computational domain for this problem is set to be $0 \leqslant x \leqslant 1$. Numerical solutions are calculated on a sequence of globally refined uniform grids and advanced in time up to $t = 10$ which corresponds to 5 periods in time.

In regions where the solution is sufficiently smooth, both the WENO and ESWENO schemes convert to a third-order linear, upwind-biased scheme with the following flux:

$$f_{j+\frac{1}{2}} = -\frac{1}{6}f_{j-1} + \frac{5}{6}f_j + \frac{1}{3}f_{j+1}. \tag{84}$$

In the vicinity of strong discontinuities and unresolved features, WENO and ESWENO schemes introduce additional nonlinear artificial dissipation through the weight functions. The presence of the nonlinear dissipation term makes these schemes more dissipative than the target third-order linear scheme (84), which provides the lower error bound that can be obtained with the WENO and ESWENO schemes for smooth solutions. The L_∞ and L_1 error norms and their convergence rates of the third-order linear, ESWENO and WENO schemes are presented in Tables 1 and 2, respectively. In Table 3, we also

Table 2
L_1 error norms and their convergence rates obtained with the third-order ESWENO, WENO, and linear schemes.

J	Linear		ESWENO		WENO	
	$\|\bar{\mathbf{u}} - \mathbf{u}_h\|_{L_1}$	Rate	$\|\bar{\mathbf{u}} - \mathbf{u}_h\|_{L_1}$	Rate	$\|\bar{\mathbf{u}} - \mathbf{u}_h\|_{L_1}$	Rate
50	6.11e−2	–	6.22e−2	–	1.02e−1	–
100	2.11e−2	1.53	2.21e−2	1.49	6.07e−2	0.75
200	3.98e−3	2.41	4.11e−3	2.42	2.28e−2	1.41
400	5.40e−4	2.88	5.42e−4	2.93	6.05e−3	1.91
800	6.84e−5	2.98	6.84e−5	2.99	1.22e−3	2.31
1600	8.58e−6	3.00	8.58e−6	3.00	1.54e−4	2.98

Table 3
L_∞ and L_1 error norms and their convergence rates obtained with the third-order WENO scheme with the new weights given by Eqs. (18) and (20)–(22).

J	$\|\bar{\mathbf{u}} - \mathbf{u}_h\|_{L_\infty}$	Rate	$\|\bar{\mathbf{u}} - \mathbf{u}_h\|_{L_1}$	Rate
50	3.86e−1	–	6.22e−2	–
100	1.63e−1	1.25	2.21e−2	1.49
200	3.67e−2	2.15	4.11e−3	2.42
400	5.19e−3	2.82	5.42e−4	2.93
800	6.33e−4	3.04	6.84e−5	2.99
1600	7.53e−5	3.07	8.58e−5	3.00

present global grid refinement results obtained with the WENO scheme whose weights are calculated by using Eqs. (18) and (20)–(22). As follows from these numerical results, the third-order ESWENO scheme significantly outperforms the conventional third-order WENO scheme in terms of accuracy and is slightly more dissipative than the WENO scheme with the new weights (18) and (20)–(22) because of the presence of the additional artificial dissipation term (48). The L_1 errors obtained with the third-order linear scheme and the ESWENO and WENO schemes with the new weights reach the design convergence rate, starting at $J = 400$ grid points, whereas the conventional WENO scheme demonstrates the design-order convergence rate only on the finest mesh with $J = 1600$.

For all grids considered, the maximum error occurs at the peak of the cosine function. As follows from Table 1, for the ESWENO scheme, the L_∞ error convergence rate is close to three on sufficiently fine meshes, thus indicating that the ESWENO scheme is third-order accurate at the smooth extremum. However, the L_∞ error norm obtained with the conventional WENO scheme exhibits only the second-order convergence rate at the finest mesh and is almost two orders of magnitude larger than that of the ESWENO scheme at $J = 1600$. The accuracy of the WENO scheme can be drastically improved and the design order can be recovered on moderate grids if the new weight functions (18) and (20)–(22) are used, as one can see in Table 3. The comparison of solutions obtained with the linear, ESWENO, and conventional WENO schemes on a 201-point grid is shown in Fig. 1. The solution of the WENO scheme with the new weights is practically indistinguishable from that of the ESWENO scheme and therefore is not presented in Fig. 1. Fig. 1 shows that the cosine pulse amplitude computed with the conventional third-order WENO scheme is much lower than those of the exact and ESWENO solutions, thus indicating that the ESWENO scheme is much less dissipative than its conventional counterpart. Another observation is that for smooth solutions, the ESWENO scheme provides practically the same accuracy as the target, linear third-order scheme.

The next question that we would like to address concerns stability of WENO and ESWENO schemes. To the authors' knowledge, no proof has been reported on the stability of WENO schemes *for problems with discontinuous solutions*. As has been discussed in Section 4, for the linear convection equation with piecewise continuous initial conditions, the ESWENO scheme is stable in the energy sense. A sufficient condition for the stability is that $-\frac{1}{2}\left(D_{\mathrm{ES}} + D_{\mathrm{ES}}^T\right)$ is negative semidefinite, where D_{ES} is the ESWENO discrete operator. This property implies that all eigenvalues of the symmetric part of the ESWENO operator are nonpositive. It should be noted that the symmetric part of the WENO operator may have positive eigenvalues as has been discussed in Section 3.2. To verify these properties, time histories of the rightmost eigenvalue of the symmetric part

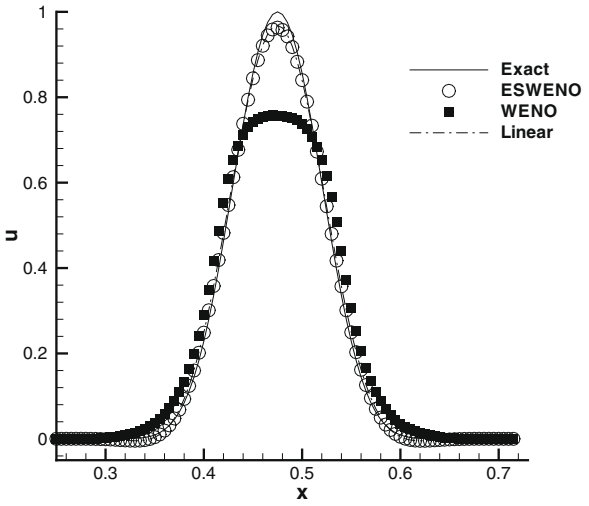

Fig. 1. Comparison of the third-order linear, ESWENO, and conventional WENO schemes for the propagation of a cosine pulse on a uniform grid with $J = 200$ over 5 time periods.

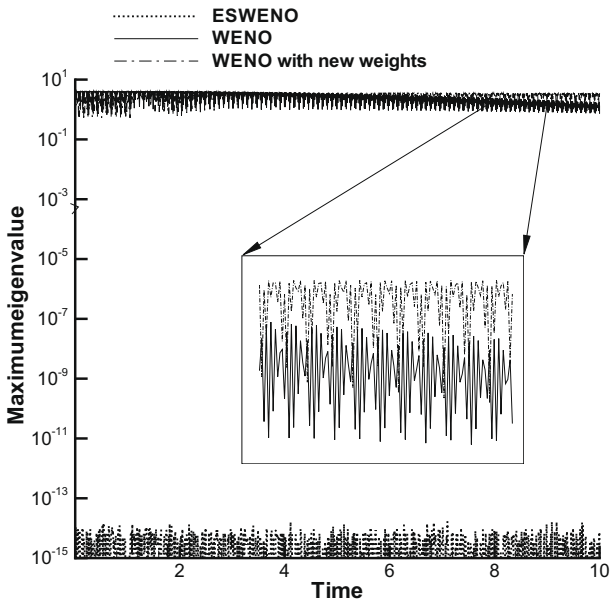

Fig. 2. Time histories of the rightmost eigenvalue of the symmetric part of the ESWENO and WENO operators.

of the ESWENO and WENO operators computed on a 101 – point grid are compared in Fig. 2. On the entire time interval considered, the maximum eigenvalue of the $-\frac{1}{2}\left(D_{\mathrm{ES}}+D_{\mathrm{ES}}^{T}\right)$ matrix is equal to zero to the order of the round-off error. In contrast to the ESWENO scheme, the symmetric part of the conventional third-order WENO operator has positive eigenvalues of the order of $O(1)$, as one can see in Fig. 2. This is due to the fact that the symmetric part of the WENO operator is not negative semidefinite, if there are unresolved features in the computational domain. As expected, the qualitative behavior of the maximum eigenvalue of the conventional WENO dissipation operator remains practically the same, regardless of the choice of the weight functions. Another important observation is that the rightmost eigenvalue of the conventional WENO operator exhibits highly oscillatory behavior. These high-amplitude oscillations indicate that the presence of eigenvalues in the right half-plane makes the conventional WENO scheme locally unstable. As a result, the WENO scheme biases the stencil away form the local instabilities caused by these eigenvalues, thus introducing additional dissipation which shifts the positive eigenvalues closer to the imaginary axis. One can see this behavior of the WENO weight functions in Fig. 3 which shows time

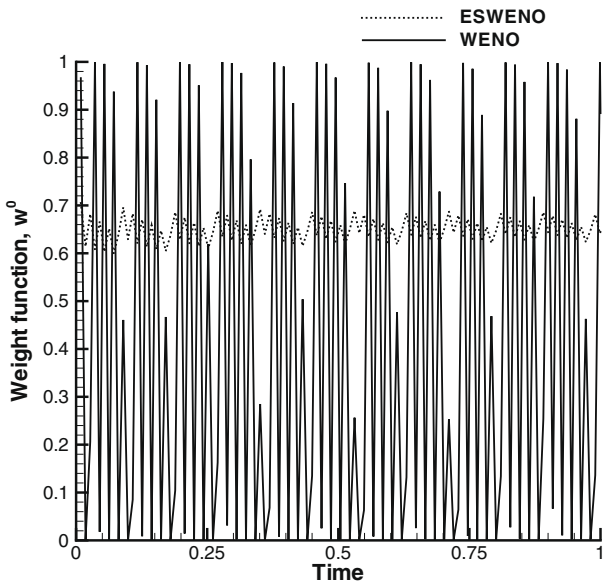

Fig. 3. Time histories of the WENO and ESWENO weight functions, w^0, at the cosine peak.

histories of the WENO and ESWENO weights, w^0, at the cosine peak. As the cosine peak, which is not fully resolved on the 101-point mesh, advances forward in the computational domain, the eigenvalues corresponding to those grid points that are in the vicinity of the unresolved feature are shifted to the right. This pattern persists over the entire time interval considered. In contrast to the WENO scheme, the ESWENO weight function, w^0, slightly oscillates and approaches to 2/3 which is its optimal value for smooth solutions. As shown in Fig. 1, for the conventional third-order WENO scheme, the presence of the unstable modes does not result in exponential growth of the solution, which is due to the dissipation mechanism of the underlying upwind-biased linear scheme. However, for central WENO schemes, whose underlying linear schemes are purely dispersive, the conventional WENO dissipation operator does not provide stability even for smooth linear convection problems, and the schemes may become globally unstable, as has been shown in [32]. The central WENO schemes can be made stable, if the ESWENO artificial dissipation term similar to Eqs. (35)–(37) is added [32], which indicates that the ESWENO dissipation mechanism plays a very important role in providing stability of the conventional WENO schemes.

The second test problem has been chosen to check whether the ESWENO scheme provides essentially non-oscillatory solutions for problems with strong discontinuities. The same linear convection Eq. (1) with $a = 0.5$ is used as a test problem. However, in contrast to the previous test case, the initial condition is set to be a piecewise continuous function given by

$$u_0(x) = \begin{cases} 1 & \text{if } |x - x_c| \leqslant \sigma, \\ 0 & \text{otherwise}, \end{cases} \tag{85}$$

where $x_c = 0.5$ and $\sigma = 0.2$. Numerical solutions obtained with the third-order linear, ESWENO, and conventional WENO schemes on a uniform grid with 101 points at time $t = 2$ are compared with the exact solution in Fig. 4. As expected, the solution computed using the linear upwind-biased scheme is oscillatory and has large-amplitude overshoots and undershoots near the discontinuities. The WENO results are free of spurious oscillations and the most dissipative among those presented in Fig. 4. The ESWENO solution is less dissipative than that obtained with the conventional WENO scheme and essentially non-oscillatory near the strong discontinuities. It should also be noted that for the test problems considered, the numerical solutions obtained with the WENO scheme with the new weights (18) and (20)–(22) are very similar to those of the ESWENO scheme and therefore are not presented hereafter.

Similar to the previous test case, we numerically analyze spectra of the symmetric part of the WENO and ESWENO finite difference operators for the linear convection Eq. (1) with the discontinuous initial condition (85). As has been shown in Sections 3.2 and 4.1, the symmetric part of the WENO operator can have positive eigenvalues, whereas the spectrum of the symmetric part of the ESWENO operator is always located in the left half-plane regardless of whether the solution is continuous or discontinuous. To verify these properties, time histories of the rightmost eigenvalue of the symmetric part of the ESWENO and WENO operators are depicted in Fig. 5. As expected, the maximum eigenvalue of $-\frac{1}{2}\left(D_{ES} + D_{ES}^T\right)$ is of the order of the machine zero. The symmetric part of the conventional WENO operator has positive eigenvalues at each time step. The largest positive eigenvalue of $-\frac{1}{2}\left(D_W + D_W^T\right)$ oscillates at the beginning and then gradually decreases, and levels out at $O(10^{-2})$. This behavior indicates that though the WENO dissipation operator tries to suppress the unstable modes, it cannot completely eliminate them. It should also be noted that for this test problem, the conventional WENO scheme is stable in the sense that the numerical solution remains bounded and does not grow exponentially.

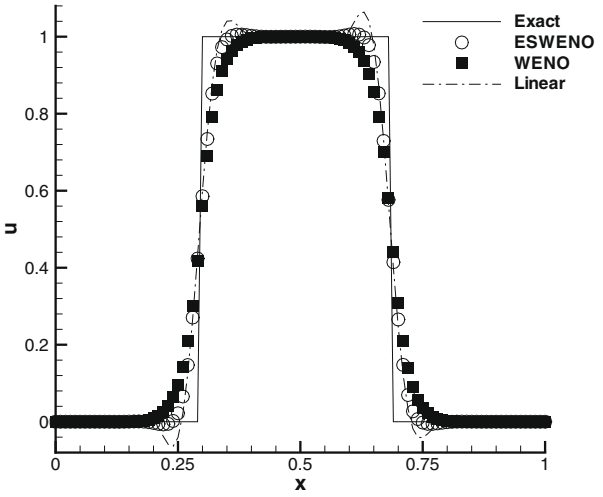

Fig. 4. Comparison of the third-order linear, ESWENO, and WENO schemes for the propagation of a square pulse on a uniform grid with $J = 100$ over 1 time period.

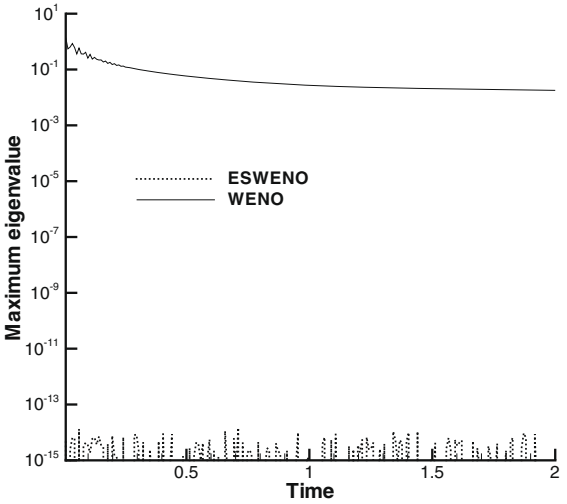

Fig. 5. Time histories of the rightmost eigenvalue of the symmetric part of the ESWENO and WENO operators.

6.2. The 1-D Euler equations

As has been proven in Section 5, the third-order ESWENO scheme is energy stable for a system of linear hyperbolic equations with periodic boundary conditions. Although there is no proof that the ESWENO scheme is stable for nonlinear systems of conservation law equations as well as for problems with nonperiodic boundary conditions, it is interesting to see how the scheme performs in this case. In connection with this, we consider the quasi-1-D Euler equations for a perfect gas, which are given by

$$\begin{aligned} &\tfrac{\partial \mathbf{U}}{\partial t} + \tfrac{\partial \mathbf{F}}{\partial x} = \mathbf{G}, \\ &\mathbf{U} = \begin{bmatrix} \rho \\ \rho u \\ E \end{bmatrix}, \quad \mathbf{F} = \begin{bmatrix} \rho u \\ \rho u^2 + p \\ (E+p)u \end{bmatrix}, \quad \mathbf{G} = -\tfrac{A_x}{A} \begin{bmatrix} \rho u \\ \rho u^2 \\ (E+p)u \end{bmatrix}, \end{aligned} \tag{86}$$

where $A = A(x)$ is the cross-sectional area of a quasi-1-D nozzle. We will first use the ESWENO and conventional WENO schemes to solve steady subsonic and transonic quasi-1-D nozzle flows and then compare solutions obtained with these schemes for essentially time-dependent problems. For the steady problems, both the ESWENO and WENO residuals were driven below 10^{-11}.

In Section 5, it has been shown that to preserve the stability of the ESWENO scheme for systems of linear hyperbolic conservation laws, the ESWENO reconstruction should be carried out in local characteristic fields, which has been implemented as recommended in [34]. First, the Roe average at $j+\frac{1}{2}$ is used to form the matrices $R_{j+\frac{1}{2}}$ and $R^{-1}_{j+\frac{1}{2}}$ composed of the left and right eigenvectors of $\partial\mathbf{F}/\partial\mathbf{U}$. Then, all quantities required to compute the ESWENO flux are multiplied by $R^{-1}_{j+\frac{1}{2}}$. After that we perform the following Lax–Friedrichs flux spitting:

$$\begin{aligned} &\mathbf{F}^{\pm} = \tfrac{1}{2}(\mathbf{F} \pm \Lambda_{\max}\mathbf{U}), \quad \Lambda_{\max} = \operatorname{diag}(\lambda^1_{\max}, \lambda^2_{\max}, \lambda^3_{\max}), \\ &\lambda^k_{\max} = \max_{0\leqslant j\leqslant J} \lambda^k_{j+\frac{1}{2}}, \quad k = \overline{1,3} \end{aligned} \tag{87}$$

and use the scalar ESWENO reconstruction for each component of the characteristics variables. Once the positive and negative ESWENO fluxes at $j+\frac{1}{2}$ have been formed, they are transformed back into the physical space by left multiplying them with $R_{j+\frac{1}{2}}$. The same local characteristic decomposition is used for the WENO scheme, but instead of the ESWENO reconstruction, the WENO reconstruction is used.

In Section 5, the stability of the ESWENO scheme has been proven only for linear hyperbolic systems that can be transformed to the characteristic fields by using a global characteristic decomposition, which is not the case for the Euler equations. No stability proof is currently available for the ESWENO scheme for the nonlinear Euler equations and the above characteristic decomposition which is done locally at each point $x_{j+1/2}$. Note, however, that for all nonlinear test problems presented hereafter, the new ESWENO scheme is stable and provides essentially nonoscillatory solutions for flows with strong shocks and contact discontinuities.

The steady state isentropic flow through a quasi-1-D nozzle with the cross-sectional area

$$A(x) = 1 - 0.8x(1-x), \quad 0 \leqslant x \leqslant 1$$

is chosen as a test problem. The inflow Mach number is set to be 0.5 and the pressure at $x = 1$ is assumed to be equal to that at $x = 0$. Under these conditions, the flow inside the nozzle is fully subsonic. Global grid refinement studies for the linear, ESWENO, and conventional WENO schemes are presented in Tables 4 and 5. As follows from this comparison, the L_∞ and L_1 error norms obtained with the ESWENO scheme are about an order of magnitude less than those of the WENO scheme and very close to their theoretical limit obtained with the third-order linear upwind-biased scheme. Note that the WENO scheme exhibits the fourth-order convergence rate on sufficiently fine meshes. This is due to the fact that on coarse meshes the WENO scheme shows only second order of convergence, while on finer meshes, the WENO scheme rapidly approaches the underlying linear scheme, thus demonstrating the rate that is greater than its asymptotic limit.

The next test problem is the steady transonic flow through a quasi-1-D nozzle with the following cross-sectional area:

$$A(x) = 1.398 + 0.347 \tanh(0.8x - 4), \quad 0 \leqslant x \leqslant 10.$$

The Mach number at $x = 0$ is 1.5, and the outflow conditions have been chosen so that the shock is located at $x = 5$. Density profiles calculated using the third-order ESWENO, conventional WENO, and linear schemes on a 51-point grid and the exact solution are shown in Fig. 6. Similar to the square pulse test problem, the numerical solution obtained with the third-order linear scheme oscillates near the shock. For both the ESWENO and WENO schemes, the captured shock is smeared over three grid cells, and the numerical solutions are essentially non-oscillatory and agree very well with the exact solution. To quantify the accuracy of each scheme in regions where the solution is smooth, we measure the L_1 error norm downstream of the shock for $x \geqslant 6$, which is presented in Table 6. As in the previous test problems considered, the ESWENO scheme is about an order of magnitude more accurate than the conventional WENO scheme on coarse and moderate grids. Note that on the coarsest 51-point mesh, the ESWENO scheme is more accurate than the target linear scheme, which is due to the presence of Gibbs oscillations in the solution obtained with the linear scheme. It is not surprising that all three schemes provide the design order of accuracy. As has been shown in [35] for the steady quasi-1D nozzle problem, the first-order error component generated by the shock-capturing procedure is localized near the shock, which is not the case for time-dependent and steady multidimensional problems [36].

To test the new ESWENO scheme for essentially unsteady flows, we first consider two classical Riemann problems of Sod and Lax. The initial conditions for the Sod problem are given by

$$(\rho, u, p) = \begin{cases} (1, 0, 1) & \text{for } 0 \leqslant x < 0.5, \\ (0.125, 0, 0.1) & \text{for } 0.5 \leqslant x \leqslant 1. \end{cases}$$

For the Lax problem, the initial distributions of the density, velocity, and pressure are

$$(\rho, u, p) = \begin{cases} (0.445, 0.698, 3.528) & \text{for } -5 \leqslant x < 0, \\ (0.5, 0, 0.571) & \text{for } 0 \leqslant x \leqslant 5. \end{cases}$$

Fig. 7 shows ESWENO, conventional WENO, and exact solutions of the Sod problem obtained at $t = 0.16$. Density profiles computed with the ESWENO and WENO schemes at $t = 1.3$ are compared with the exact solution of the Lax problem in Fig. 8. Similar to all previous test problems, the ESWENO scheme is more accurate than the standard WENO scheme of Jiang and Shu and provides better resolution of the contact discontinuities and the shock waves, while maintaining the ENO property.

Table 4
L_∞ error norms and their convergence rates obtained with the third-order linear, ESWENO and conventional WENO schemes for the subsonic quasi-1-D nozzle problem.

J	Linear		ESWENO		WENO	
	$\|\bar{\mathbf{u}} - \mathbf{u}_h\|_{L_\infty}$	Rate	$\|\bar{\mathbf{u}} - \mathbf{u}_h\|_{L_\infty}$	Rate	$\|\bar{\mathbf{u}} - \mathbf{u}_h\|_{L_\infty}$	Rate
50	7.04e−6	–	9.63e−6	–	6.70e−3	–
100	8.55e−7	3.04	1.15e−6	3.05	9.94e−5	2.75
200	1.05e−7	3.03	1.41e−7	3.02	6.25e−6	3.99
400	1.30e−8	3.01	1.75e−8	3.01	3.73e−7	4.07
800	1.62e−9	3.01	2.18e−9	3.01	2.01e−8	4.22

Table 5
L_1 error norms and their convergence rates obtained with the third-order linear, ESWENO and conventional WENO schemes for the subsonic quasi-1-D nozzle problem.

N	Linear		ESWENO		WENO	
	$\|\bar{\mathbf{u}} - \mathbf{u}_h\|_{L_1}$	Rate	$\|\bar{\mathbf{u}} - \mathbf{u}_h\|_{L_1}$	Rate	$\|\bar{\mathbf{u}} - \mathbf{u}_h\|_{L_1}$	Rate
50	2.79e−6	–	3.59e−6	–	9.57e−5	–
100	3.40e−7	3.04	4.33e−7	3.05	1.27e−5	2.92
200	4.19e−8	3.02	5.32e−8	3.02	1.24e−6	3.35
400	5.19e−9	3.01	6.60e−9	3.01	1.02e−7	3.61
800	6.47e−10	3.01	8.21e−10	3.01	6.87e−9	3.89

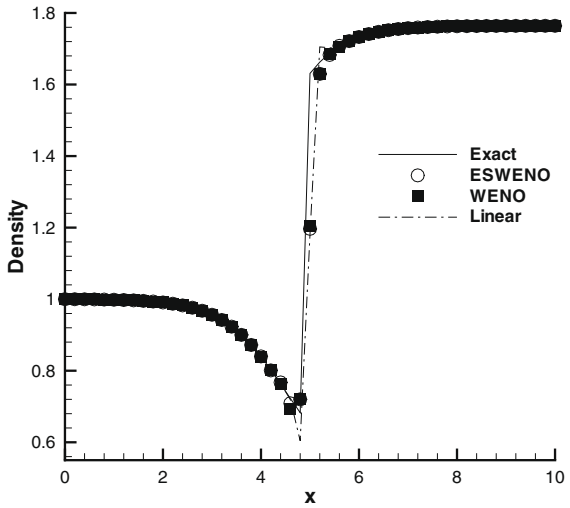

Fig. 6. Comparison of the third-order ESWENO, WENO, and linear schemes for the steady transonic flow through the quasi-1-D nozzle.

Table 6
L_1 error norms and their convergence rates measured downstream of the shock for $x \geqslant 6$, which were computed using the linear, ESWENO and WENO schemes for the transonic quasi-1-D nozzle problem.

J	Linear		ESWENO		WENO	
	$\|\|\bar{\mathbf{u}} - \mathbf{u}_h\|\|_{L_1}$	Rate	$\|\|\bar{\mathbf{u}} - \mathbf{u}_h\|\|_{L_1}$	Rate	$\|\|\bar{\mathbf{u}} - \mathbf{u}_h\|\|_{L_1}$	Rate
50	2.06e−5	–	1.37e−5	–	1.36e−4	–
100	9.83e−7	4.39	1.41e−6	3.28	1.57e−5	3.11
200	1.19e−7	3.04	1.71e−7	3.04	1.53e−6	3.36
400	1.47e−8	3.02	2.10e−8	3.03	1.13e−7	3.75
800	1.82e−9	3.01	2.60e−9	3.01	6.90e−9	4.04

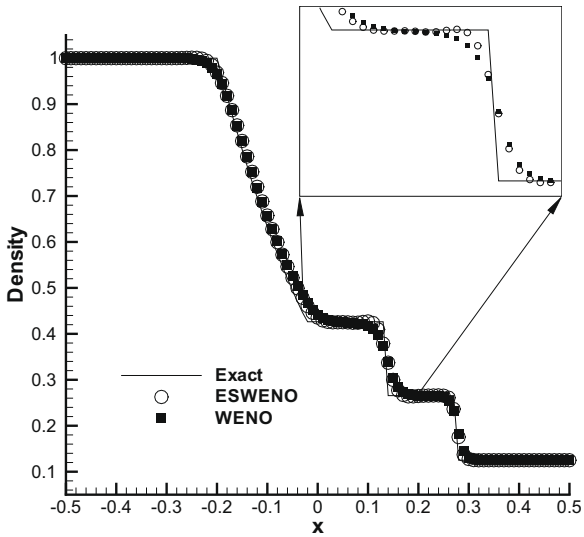

Fig. 7. Density profiles computed with the 3-rd-order ESWENO and conventional WENO schemes on a uniform grid with 101 points for the Sod problem.

The next test problem, which was originally proposed by Woodward and Colella, has been chosen to evaluate the performance of the third-order ESWENO scheme for flows with very strong shocks and contact discontinuities. For this problem, the initial conditions are

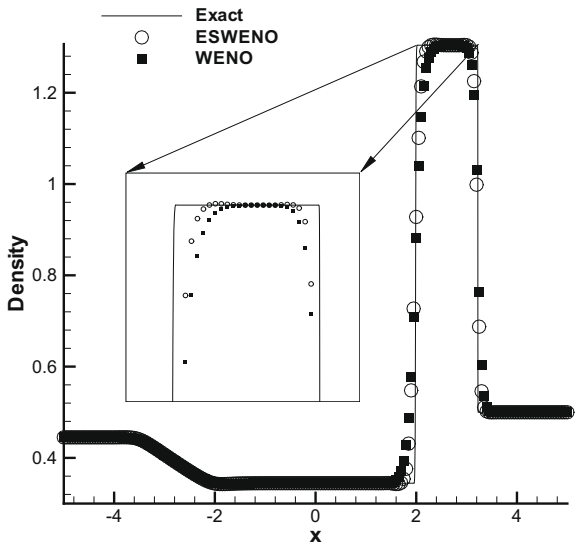

Fig. 8. Density profiles computed with the 3-rd-order ESWENO and conventional WENO schemes on a uniform grid with 201 points for the Lax problem.

$$(\rho,u,p)=\begin{cases}(1,0,1000) & \text{for } 0\leqslant x<0.1,\\ (1,0,0.01) & \text{for } 0.1\leqslant x\leqslant 0.9,\\ (1,0,100) & \text{for } 0.9\leqslant x\leqslant 1\end{cases}$$

and the reflection boundary conditions are imposed on both the left and right boundaries. Fig. 9 compares the ESWENO and WENO density distributions at $t=0.038$ with the reference solution computed by the third-order WENO scheme on a uniform grid with $J=10000$ cells. As before, the physical extrema at $x=0.647,\ 0.748,\ 0.777$ and the contact discontinuities at $x=0.594$ and 0.765 of the ESWENO solution are much better resolved as compared with those of the conventional WENO counterpart.

The last test problem considered is the interaction of a moving shock with smooth density fluctuations. The solution of this benchmark problem contains both strong discontinuities and smooth structures, which is very well suited for testing high-order shock-capturing schemes. The governing equations are the time-dependent 1-D Euler Eq. (86) with $\mathbf{G}=\mathbf{0}$, subject to the following initial conditions:

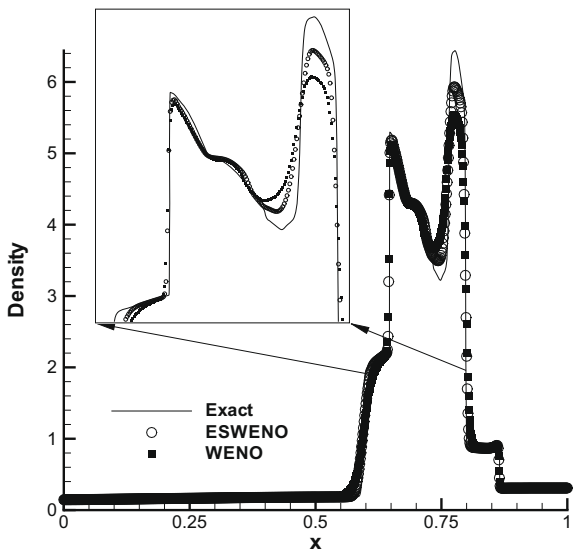

Fig. 9. Density profiles computed with the 3-rd-order ESWENO and conventional WENO schemes on a uniform grid with 801 points for the Woodward and Colella problem.

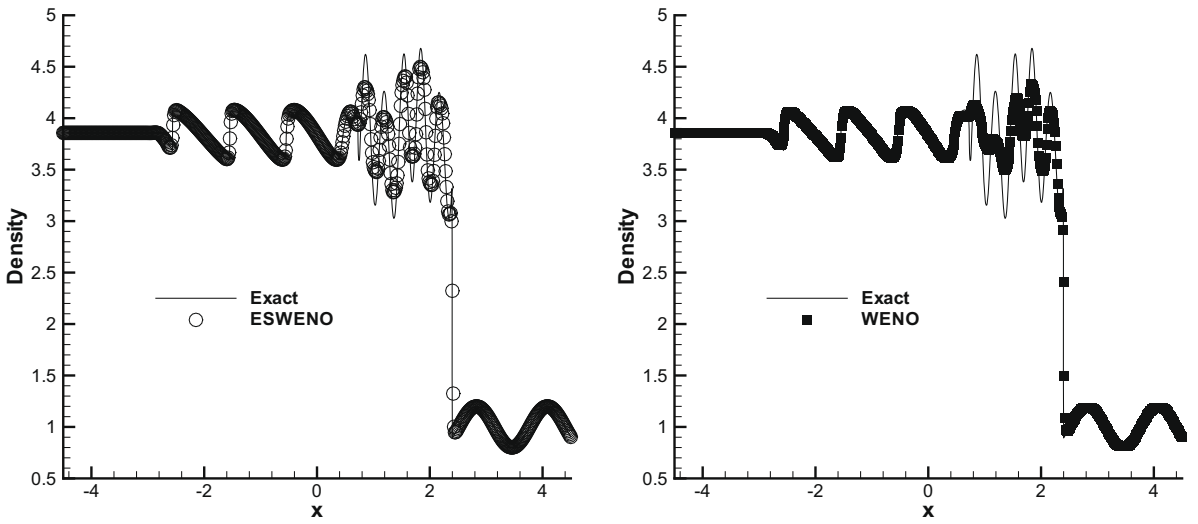

Fig. 10. Density profiles computed with the 3-rd-order ESWENO (left) and conventional WENO (right) schemes on a uniform grid with 601 points for the density sine wave/shock interaction problem.

$$(\rho, u, p) = \begin{cases} (3.857134, 2.629369, 10.33333) & \text{for } -5 \leqslant x < -4, \\ (1 + 0.2\sin 5x, 0, 1) & \text{for } -4 \leqslant x \leqslant 5. \end{cases}$$

The governing equations are integrated in time up to $t = 1.8$. The exact solution to this problem is not available. Therefore, a numerical solution obtained with the conventional third-order WENO scheme on a uniform grid with $J = 10000$ grid cells is used as a reference solution.

The parameters ϵ and δ for the ESWENO scheme are given by Eqs. (65) and (66), which have been used for all previous test problems. The local characteristic decomposition based on the global Lax–Friedrichs flux splitting (87) is used for both the ESWENO and WENO reconstructions. Numerical solutions obtained with the third-order ESWENO and conventional WENO schemes on a 601-point grid at $t = 1.8$ are compared with the "exact" reference solution in Fig. 10.

Note that both the ESWENO and WENO solutions are free of spurious oscillations. Fig. 10 shows that the third-order ESWENO scheme is more accurate than its conventional counterpart and provides much better resolution in a region right upstream of the moving shock. As has been discussed above, two major factors that make the conventional WENO scheme too dissipative are the choice of the weight functions and the presence of positive eigenvalues in the spectrum of the symmetric part of the WENO operator.

7. Conclusions

A new third-order ESWENO finite difference scheme is developed for scalar and vector linear hyperbolic equations with discontinuous solutions. The new scheme combines the standard third-order WENO scheme and an additional nonlinear artificial dissipation term. The additional term is third-order accurate for smooth solutions. This term guarantees that the new scheme is stable in the L_2-energy norm for both continuous and discontinuous solutions, whereas for the conventional WENO scheme, an energy estimate is not available. The distinctive feature of the ESWENO scheme is that the stability has been proven for any form of weight functions that satisfy Eq. (23). We have also constructed new weight functions which provide much faster convergence of the WENO and ESWENO schemes to the underlying third-order upwind-biased linear scheme. The turning parameters ϵ and δ of the ESWENO scheme have been chosen based on the truncation error analysis, which guarantee design-order accuracy for smooth solutions with any number of vanishing derivatives. The spectrum of the symmetric part of the ESWENO operator is always located in the left half-plane, whereas the symmetric part of the WENO operator has positive eigenvalues, thus indicating that the WENO scheme may become locally unstable. The numerical experiments have shown that the ESWENO scheme with the new weights is much more accurate than the conventional WENO scheme of Jiang and Shu in regions where the solution is smooth and provides essentially non-oscillatory solutions near strong discontinuities and unresolved features.

Acknowledgement

The work of the first author was supported in part by the Army Research Laboratory under Grant W911NF-06-R-006.

References

[1] A. Harten, B. Engquist, S. Osher, S. Chakravarthy, Uniformly high order essentially non-oscillatory schemes, III, J. Comput. Phys. 71 (1987) 231–303.
[2] X.-D. Liu, S. Osher, T. Chan, Weighted essentially non-oscillatory schemes, J. Comput. Phys. 115 (1994) 200–212.
[3] G. Jiang, C.-W. Shu, Efficient implementation of weighted ENO schemes, J. Comput. Phys. 126 (1996) 202–228.
[4] Z.J. Wang, R.F. Chen, Optimized weighted essentially non-oscillatory schemes for linear waves with discontinuity, J. Comput. Phys. 174 (2001) 381–404.
[5] M.P. Martin, E.M. Taylor, M. Wu, V.G. Weris, A bandwidth-optimized WENO scheme for the effective direct numerical simulation of compressible turbulence, J. Comput. Phys. 220 (2006) 270–289.
[6] D. Balsara, C.-W. Shu, Monotonicity preserving weighted essentially non-oscillatory schemes with increasingly high order of accuracy, J. Comput. Phys. 160 (2000) 405–452.
[7] D. Levy, G. Puppo, G. Russo, Compact central WENO schemes for multidimensional conservation laws, SIAM J. Sci. Comput. 22 (2) (2000) 656–672.
[8] J. Casper, H.L. Atkins, A finite-volume high-order scheme for 2-dimensional hyperbolic systems, J. Comput. Phys. 106 (1993) 62–76.
[9] O. Friedrichs, Weighted essentially non-oscillatory schemes for the interpolation of mean values on unstructured grids, J. Comput. Phys. 144 (1998) 194–212.
[10] C. Hu, C.-W. Shu, Weighted essentially non-oscillatory schemes on triangular meshes, J. Comput. Phys. 150 (1999) 92–127.
[11] J. Qiu, C.-W. Shu, Runge–Kutta discontinuous Galerkin method using WENO limiters, SIAM J. Sci. Comput. 26 (3) (2005) 907–929.
[12] H. Luo, J.D. Baum, R. Löhner, A Hermite WENO-based limiter for discontinuous Galerkin method on unstructured grids, J. Comput. Phys. 225 (2007) 686–713.
[13] G. Jiang, S.-H. Yu, Discrete shocks for finite difference approximations to scalar conservation laws, SIAM J. Numer. Anal. 35 (2) (1998) 749.
[14] R. Ferretti, Convergence of semi-Lagrangian approximations to convex Hamilton–Jacobi equations under (very) large Courant numbers, SIAM J. Numer. Anal. 40 (6) (2003) 2240–2253.
[15] J.-M. Qiu, C.-W. Shu, Convergence of Godunov-type schemes for scalar conservation laws under large time steps, SIAM J. Numer. Anal. 46 (2008) 2211.
[16] S. Osher, E. Tadmor, On the convergence of the difference approximations to scalar conservation laws, Math. Comput. 50 (1988) 19–51.
[17] H. Yang, On wavewise entropy inequality for high resolution schemes II: fully discrete MUSCL schemes with exact evolution in small time, SIAM J. Numer. Anal. 36 (1) (1998) 1–31.
[18] G. Jiang, C.-W. Shu, On a cell-entropy inequality for discontinuous Galerkin methods, Math. Comput. 62 (1994) 531–538.
[19] S. Hou, X.-D. Liu, Solutions of multi-dimensional hyperbolic systems of conservation laws by square entropy condition satisfying discontinuous Galerkin method, J. Sci. Comput. 31 (2007) 127–151.
[20] H.O. Kreiss, G. Scherer, Finite element and finite difference methods for hyperbolic partial differential equations, Mathematical Aspects of Finite Elements in Partial Differential Equations, Academic Press, New York, 1974.
[21] B. Strand, Summation by parts for finite difference approximations for d/dx, J. Comput. Phys. 110 (1) (1994) 47.
[22] M.H. Carpenter, D. Gottlieb, S. Abarbanel, Time-stable boundary conditions for finite difference schemes solving hyperbolic systems: methodology and application to high-order compact schemes, J. Comput. Phys. 111 (2) (1994).
[23] K. Mattsson, M. Svärd, J. Nordström, Stable and accurate artificial dissipation, J. Sci. Comput. 21 (1) (2004) 57–79.
[24] M.H. Carpenter, D. Gottlieb, Spectral methods on arbitrary grids, J. Comput. Phys. 129 (1996) 74–86.
[25] J.S. Hesthaven, D. Gottlieb, A stable penalty method for the compressible Navier–Stokes equations: I. open boundary conditions, SIAM J. Sci. Comput. 17 (3) (1996) 579–612.
[26] M.H. Carpenter, J. Nordström, D. Gottlieb, A stable and conservative interface treatment of arbitrary spatial accuracy, J. Comput. Phys. 148 (1999) 341–365.
[27] R. Borges, M. Carmona, B. Costa, W.S. Don, An improved weighted essentially non-oscillatory scheme for hyperbolic conservation laws, J. Comput. Phys. 227 (2008) 3191–3211.
[28] A.K. Hendrick, T.D. Aslam, J.M. Powers, Mapped weighted essentially non-oscillatory schemes: achieving optimal order near critical points, J. Comput. Phys. 207 (2005) 542–567.
[30] P.D. Lax, B. Wendroff, Systems of conservation laws, Commun. Pure Appl. Math. 13 (1960) 217.
[31] C.-W. Shu, Total-variation-diminishing time discretizations, SIAM J. Sci. Stat. Comput. 9 (1988) 1073.
[32] N.K. Yamaleev, M.H. Carpenter, A systematic methodology for constructing high-order energy stable WENO schemes, NASA TM 2008-215532, 2008.
[33] J. Qiu, C.-W. Shu, On the construction, comparison, and local characteristic decomposition for high-order central WENO schemes, J. Comput. Phys. 183 (2002) 187–209.
[34] C.-W. Shu, Essentially non-oscillatory and weighted essentially non-oscillatory schemes for hyperbolic conservation laws, in: B. Cockburn, C. Johnson, C.-W. Shu, E. Tadmor (Eds.), Advanced Numerical Approximation of Nonlinear Hyperbolic Equations, in: A. Quarteroni (Ed.), Lecture Notes in Mathematics, vol. 1697, Springer, 1998, pp. 325–432.
[35] M.B. Giles, Analysis of the accuracy of shock-capturing in the steady quasi-1D Euler equations, Comput. Fluid Dynam. J. 5 (2) (1996) 247–258.
[36] M.H. Carpenter, J. Casper, Accuracy of shock capturing in two spatial dimensions, AIAA J. 37 (1999) 1072–1079.